Alfvén Waves at Mars

N. Romanelli[1,2,*], C. M. Fowler[3], G. A. DiBraccio[2], J. R. Espley[2], J. S. Halekas[4]

(1) Department of Astronomy, University of Maryland, College Park, MD, USA.
(2) Planetary Magnetospheres Laboratory, NASA Goddard Space Flight Center, Greenbelt, MD, USA.
(3) Department of Physics and Astronomy, West Virginia University, Morgantown, WV, USA.
(4) Department of Physics and Astronomy, University of Iowa, Iowa City, IA, USA.

(*) Corresponding author: norberto.romanelli@nasa.gov

arXiv:2403.17304v1 [astro-ph.SR] 26 Mar 2024

Abstract

The solar wind upstream of Mars's bow shock can be described in terms of Alfvénic turbulence, with an incompressible energy cascade rate of 10^{-17} J m^{-3} s^{-1} at magnetohydrodynamics (MHD) scales. The solar wind has more Alfvén waves propagating outwards from the Sun (than inwards) and a median Alfvén ratio of ~ 0.33. Newly ionized planetary protons associated with the extended hydrogen corona generate waves at the local proton cyclotron frequency. These 'proton cyclotron waves' (PCW) mostly correspond to fast magnetosonic waves, although the ion cyclotron (Alfvénic) wave mode is possible for large Interplanetary Magnetic Field cone angles. PCW do not show significant effects on the solar wind energy cascade rates at MHD scales but could affect smaller scales. The magnetosheath displays high amplitude wave activity, with high occurrence rate of Alfvén waves. Turbulence appears not fully developed in the magnetosheath, suggesting fluctuations do not have enough time to interact in this small-size region. Some studies suggest PCW affect turbulence in the magnetosheath. Overall, wave activity is reduced inside the magnetic pile-up region and the Martian ionosphere. However, under certain conditions, upstream waves can reach the upper ionosphere. So far, there have not been conclusive observations of Alfvén waves in the ionosphere or along crustal magnetic fields, which could be due to the lack of adequate observations.

1 Introduction

More than eighty years ago, Hannes Alfvén proposed the existence of a new type of electromagnetic-hydrodynamic wave capable of propagating in a conductive fluid medium (Alfvén, 1942). Cur-

rently known as Alfvén waves, they are the result of the coupling between the plasma motion and magnetic field line stresses. Plasma flow across magnetic field lines bends them, perturbing the current density field, modifying the total magnetic field force, and ultimately affecting plasma motion itself. Alfvén waves, fast and slow magnetosonic waves, are the three low-frequency normal modes present in a magnetized ideal conductive fluid medium, whose evolution over long time scales, is described by means of magnetohydrodynamics or MHD theory (e.g., Cramer, 2001). In the MHD regime, the Alfvén wave mode is incompressible, not presenting perturbations in the plasma density and particle pressure. The magnetic field strength is also unaffected by this normal wave mode. Identifying wave modes is important as, under many conditions, they constitute a non-collisional coupling in space and astrophysical plasmas. Moreover, this identification also allows us to indirectly infer other physical processes occurring in a variety of environments, such as the solar wind and the magnetospheres of planets (e.g., Kivelson and Russell, 1995).

The pristine solar wind upstream from Mars has been studied in terms of incompressible Alfvénic turbulence (Parker, 1958; Pope, 2001). Nonlinear wave activity is modeled in terms of the interaction of counter-streaming Alfvén waves and by the presence of an inertial range, where energy is transferred without dissipation throughout several spatial and temporal scales (e.g., Frisch, 1995; Bruno and Carbone, 2013; Andrés et al., 2020). In the MHD scales, the magnetic field power spectral density displays a Kolmogorov-like form. In this regime, the power of magnetic field fluctuations follows a power law with the wave frequency, and the spectral index is equal to -5/3 (e.g., Alexandrova, 2008; Ruhunusiri et al., 2017; Andrés et al., 2020).

The interaction between the magnetized solar wind and the Martian ionosphere contributes to a planetary magnetosphere that bears similarities with those of Venus and comets (e.g., Acuña et al., 1998; Acuña et al., 1999; Mazelle et al., 2004; Nagy et al., 2004; Halekas et al., 2021; Cravens and Gombosi, 2004; Bertucci et al., 2011; Dubinin et al., 2023). On the other hand, the presence of crustal magnetic fields and the interaction with the Interplanetary Magnetic Field (IMF) is responsible for features also present in intrinsically magnetized planetary magnetospheres. In particular, crustal magnetic fields create mini-magnetospheres, with characteristics that resemble those of magnetized planets but at localized scales; they can magnetically reconnect with the solar wind IMF, providing the solar wind access to localized regions of the ionosphere (in analogy to the cusp regions at Earth); and contribute to the dynamics of the environment. Indeed, crustal magnetic fields rotate with the planet, adding to the proper solar

wind variability (e.g., Acuña et al., 1998; Acuña et al., 1999; Brain et al., 2003; Harada et al., 2018; DiBraccio et al., 2022; Bowers et al., 2023). As a result, the interaction between the solar wind/IMF, the Martian ionosphere, and the remanent crustal magnetic fields results in a hybrid planetary magnetosphere (e.g., DiBraccio et al., 2022; Dubinin et al., 2023).

The first boundary the solar wind encounters when interacting with the Martian magnetosphere is the bow shock, as shown in Figure 1. Electromagnetic forces in this collisionless boundary slow down and heat the incoming supermagnetosonic solar wind. As the upstream solar wind Alfvén Mach number is high at Mars heliocentric distances ($M_A \sim 11$), backstreaming protons are generated, which contribute to diverting the solar wind around the planet (Halekas et al., 2017; Slavin and Holzer, 1981; Edmiston and Kennel, 1984; Paschmann et al., 1980; Sonnerup, 1969; Biskamp, 1973; Gosling and Robson, 1985; Phillips and Robson, 1972). Thus, a foreshock is present at Mars under nominal solar wind conditions (Eastwood et al., 2005; Jarvinen et al., 2022; Burgess et al., 2005; Bale et al., 2005). The backstreaming protons interact with the incoming solar wind and give rise to low-frequency waves immersed in the Martian foreshock (e.g., Meziane et al., 2017; Romanelli et al., 2018a; Jarvinen et al., 2022). In addition, the shock generates electromagnetic plasma waves capable of overcoming the solar wind velocity and traveling upstream (e.g., Mazelle et al., 2004). The average bow shock stand-off distance is $\sim 1.6R_M$, where $1R_M \sim 3390$ km, significantly smaller relative to those associated with intrinsically magnetized planets (e.g., Mazelle et al., 2004; Gruesbeck et al., 2018; Eastwood et al., 2005; Turc et al., 2023). For instance, the average Earth's bow shock stand-off distance is $\sim 14R_E$, where R_E stands for Earth's radius ($1R_E \sim 6378$ km) (e.g., Fairfield, 1971; Formisano, 1979).

The region downstream of the bow shock, the magnetosheath, is characterized by compressed, heated, and slower solar wind plasma and high-amplitude wave activity (e.g., Halekas et al., 2017; Halekas, 2017; Fowler et al., 2017). The sources of these waves are numerous, from transmission through the bow shock, to local generation to energy transfer between modes and scales (e.g., Dubinin and Fraenz, 2016; Ruhunusiri et al., 2017). The inner boundary of the magnetosheath is the magnetic pile-up boundary or MPB, whose average stand-off distance is $\sim 1.2\,R_M$. Dowstream from the MPB, the background magnetic field drapes and piles up around Mars (e.g., Trotignon et al., 2006; Bertucci et al., 2011; Romanelli et al., 2014; Espley, 2018). Moreover, the plasma is mostly composed of planetary heavy ions and the magnetic field strength is generally larger than in the magnetosheath, resulting in a region of relatively

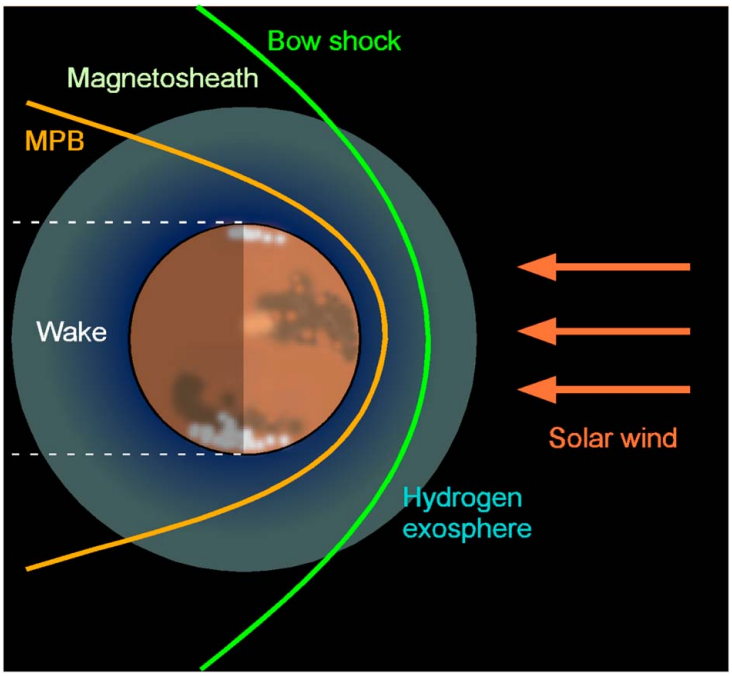

Figure 1: Schematic representation of the Martian magnetosphere. The bow shock is the boundary that separates the upstream solar wind from the magnetosheath region. It contributes to solar wind heating and deceleration. The magnetic pileup boundary (or MPB) is the inner boundary that separates the magnetosheath from the magnetic pileup region. Downstream of the MPB, the plasma is mostly composed of planetary heavy ions. Due to Mars' relatively weak gravity field and the lack of an intrinsic global magnetic field, the hydrogen corona extends beyond Mars's bow shock. Source: Taken from Ruhunusiri et al. (2017).

dense and low plasma beta and generally less intense wave activity (Nagy et al., 2004; Fowler et al., 2017). Additionally, Mars also has a magnetotail consisting of magnetic lobes of opposite polarity separated by a current sheet whose location depends on the IMF (e.g., Crider et al., 2004; Romanelli et al., 2015, 2018b; Harada et al., 2015; DiBraccio et al., 2017, 2018, 2022; Ramstad et al., 2020; Curry et al., 2022). A significant fraction of the total planetary ion escape occurs down the magnetotail region, with particle fluxes dependent on position, particle energy, and external conditions (such as the orientation of the IMF), among other parameters (e.g., Dubinin et al., 2011; Curry et al., 2022).

Mars also has a hydrogen (H) exosphere that extends beyond the bow shock (Bhattacharyya et al., 2015; Chaffin et al., 2015). This is due to Mars's relatively weak gravity and small size magnetosphere due, in turn, to the lack of a global intrinsic magnetic field (Acuña et al., 1998). The neutral exospheric atoms are ionized by photoionization, charge exchange, and electron impact, and give rise to a newborn planetary proton population, initially nearly at rest with respect to Mars (Yamauchi et al., 2015; Rahmati et al., 2015, 2017). Seasonal variability of the H corona results in seasonal variability of the newborn planetary proton population,

also creating seasonal variability in physical processes occurring inside and upstream of the magnetosphere of Mars. In particular, previous studies have reported seasonal and long-term variability of low-frequency wave activity upstream of Mars and effects inside the magnetosphere (e.g., Bhattacharyya et al., 2015; Yamauchi et al., 2015; Ruhunusiri et al., 2017; Halekas, 2017; Romanelli et al., 2016; Romeo et al., 2021; Hughes et al., 2019; Halekas et al., 2020; Jiang et al., 2023).

In addition, the relatively small scale size of the Martian magnetosphere means that characteristic length scales of the plasma (such as the proton gyro radius) are comparable to the length scales of the system (e.g. bow shock stand-off distance), implying that the shocked solar wind does not have space to fully thermalize before encountering the planet. Kinetic effects are thus likely to play a key role in the Mars - solar wind interaction (e.g., Moses et al., 1988; Kallio et al., 2011; Dong et al., 2015; Romanelli et al., 2019; Jarvinen et al., 2022). In particular, although some of the observed wave properties may be understood in terms of MHD normal modes, previous analyses have shown statistical and case studies where wave polarization and frequency and the local ion and electron velocity distribution functions necessarily demand a kinetic description. This is the case, for instance, for most ultra-low frequency (ULF) waves observed upstream from the Martian bow shock and in the foreshock. The observed polarization is typically elliptical or circular, while MHD predicts linearly polarized modes. Moreover, particle populations in these regions are far from Maxwellians (e.g., Russell, 1994; Mazelle et al., 2004; Romanelli et al., 2016; Meziane et al., 2017; Romeo et al., 2021; Jarvinen et al., 2022). It is also worth mentioning that the presence of boundaries (bow shock and MPB) affects the possible wave modes excited in the Martian magnetosphere. Examples of associated processes are mode conversion, wave reflection as well as surface waves, among others.

The relatively small size of the hybrid Martian magnetosphere also suggests that waves resulting from the interaction with the solar wind should be present downstream of the bow shock and even in the ionosphere. Subsequent observations have confirmed that this is the case and the magnetosphere of Mars is now known to be a highly dynamic environment, where processes taking place upstream from the bow shock can significantly impact the underlying ionosphere (e.g., Halekas et al., 2017; Fowler et al., 2017; Ruhunusiri et al., 2017; Jiang et al., 2023). Studying the electromagnetic wave environment at Mars is thus very important as waves can facilitate energy propagation and transfer in the collisionless environment, heat the ionosphere and potentially modify planetary ion escape (e.g., Ergun et al., 2006; Fowler et al., 2018a;

Collinson et al., 2018; Jarvinen et al., 2022). Furthermore, waves can lead or modify magnetic field reconnection conditions in the Martian magnetosphere (Chen et al., 2022; Bowers et al., 2023). In other words, the presence of an extended H exosphere, the relatively small size of the Martian magnetosphere, and the remanent crustal magnetic fields, among other parameters, provide a compelling plasma environment in the solar system to study electromagnetic plasma wave generation and evolution.

Different planetary missions to Mars have allowed the identification of several low-frequency waves. The first observations of wave activity at Mars were obtained by the Phobos-2 mission (e.g., Grard et al., 1989; Russell et al., 1990; Skalsky et al., 1998; Delva and Dubinin, 1998). Since then, analysis of magnetic, electric, and plasma observations by Phobos-2, Mars Global Surveyor (MGS), Mars EXpress (MEX), and Mars Atmosphere and Volatile EvolutioN (MAVEN) missions to Mars presented us with a picture where certain types of waves are more likely to be observed in different regions of the Martian magnetosphere and upstream, with variability in their properties and occurrence rate. Despite this progress, comprehensive analysis of low-frequency waves in the Martian magnetosphere has been limited for several reasons. The Phobos-2 mission had a relatively high periapsis ($\sim$ 900 km) and lasted $\sim$ 8.5 months, resulting in a relatively small amount of data. MGS lacked an ion instrument capable of measuring the bulk properties of local plasma. Additionally, most of its orbits were Sun-synchronous at $\sim$ 400 km, affecting the spatial coverage of the Martian magnetosphere throughout this mission (11 September 1997 - 2 November 2006). Since 25 December 2003, MEX has explored the Martian magnetosphere, providing valuable measurements that continue to improve our understanding of plasma processes. However, the lack of a magnetometer onboard MEX puts constraints on the characterization of wave modes around Mars. Inserted into orbit around Mars on 21 September 2014, MAVEN is the first and only spacecraft so far to observe all main regions of the magnetosphere carrying a magnetometer, an ion plasma analyzer, and an electric field instrument. Moreover, its precessing orbit also allows sampling of the entire magnetosphere under different solar wind and solar cycle conditions (Jakosky et al., 2015).

In this Chapter, we provide a review focused on Alfvén waves, taking into account the presence of other wave modes. Several excellent reviews on low-frequency waves at Mars provide a comprehensive context for this work (Russell, 1994; Mazelle et al., 2004; Glassmeier and Espley, 2006; Delva et al., 2011; Dubinin and Fraenz, 2016). This Chapter is centered on and highlights some of the many recent observations and conclusions provided by the ongoing MAVEN mission

(Jakosky et al., 2015).

2 Alfvén waves upstream from the Martian Bow Shock

Alfvén waves of several wavelengths are present in the upstream solar wind. These waves are responsible for correlated fluctuations in the magnetic and velocity fields, which can affect the Martian plasma environment (Belcher and Davis, 1971; Halekas et al., 2017; Andrés et al., 2020). In addition, the nonlinear interaction between counter-streaming Alfvén waves is considered to be responsible for the energy cascade, by which energy is transferred throughout several scales of the system. Under many conditions, the sense of the nonlinear energy transfer is directed from the larger wavelengths (or timescales) to the smaller ones. This is the so-called direct incompressible energy cascade of the solar wind (Bruno and Carbone, 2013; Alexandrova, 2008; Maron and Goldreich, 2001; Ruhunusiri et al., 2017; Andrés et al., 2020; Romanelli et al., 2022).

A study conducted by Halekas et al. (2017) made use of 45 s average MAVEN Magnetometer (MAG) and Solar Wind Ion Analyzer (SWIA) observations to study the Alfvénic content in the Martian magnetosphere and upstream of the bow shock (Connerney et al., 2015; Halekas et al., 2015). Among the explored properties, the authors computed the normalized cross-helicity σ_C, the normalized residual energy σ_r, and the Alfvén ratio, defined as follows:

$$\sigma_C = \frac{2\,\langle \delta\mathbf{u} \cdot \delta\mathbf{u}_A \rangle}{\langle \delta\mathbf{u}^2 + \delta\mathbf{u}_A^2 \rangle} \tag{1}$$

$$\sigma_r = \frac{\langle \delta\mathbf{u}^2 - \delta\mathbf{u}_A^2 \rangle}{\langle \delta\mathbf{u}^2 + \delta\mathbf{u}_A^2 \rangle} \tag{2}$$

$$r_A = \frac{\langle \delta\mathbf{u}^2 \rangle}{\langle \delta\mathbf{u}_A^2 \rangle} \tag{3}$$

where $\delta\mathbf{u}$ and $\delta\mathbf{u}_A$ are the solar wind bulk and Alfvén incompressible velocity fluctuations, respectively. The latter is defined as $\mathbf{u}_A \equiv \mathbf{B}/\sqrt{\mu_0\rho_0}$, where ρ_0 is the mean mass plasma density and μ_0 is the vacuum magnetic permeability. The angular bracket $\langle\rangle$ indicates a time average over each 30-minute analyzed interval. Note that, by definition, $-1 \leq \sigma_C \leq 1$, $-1 \leq \sigma_r \leq 1$, and $r_A \geq 0$.

The normalized cross-helicity σ_C is a measure of the linear correlation between velocity and magnetic field fluctuations. A value of $\sigma_C = \pm 1$ is consistent with an Alfvén wave propagating antiparallel or parallel to the background magnetic field direction. Usually, fluctuations with $|\sigma_C| \sim 1$ are described as Alfvénic. The normalized residual energy and the Alfvén ratio quantify the energy balance between the kinetic and magnetic field fluctuations. In particular, a value of $\sigma_r = 0$ is consistent with energy equipartition, and values of $\sigma_r < 0$ show a given event has more energy in the magnetic field fluctuations. Consistently, a value of $r_A = 0$ implies all energy is present in the magnetic field fluctuations and $r_A = 1$ is associated with energy equipartition.

Halekas et al. (2017) showed that the solar wind upstream from the Martian bow shock has a majority of Alfvén waves that propagate outward from the Sun. Figure 2a-c displays a larger amount of waves with negative (positive) normalized cross-helicities for +By/-Bx (-By/+Bx) Mars Solar Orbital (MSO) IMF configuration (Roberts et al., 1987). The MSO coordinate system is centered on Mars with the X-axis pointing toward the Sun, and the Z-axis perpendicular to Mars's orbital plane and positive towards the ecliptic north. The Y-axis completes the right-handed system. Moreover, Figure 2d also shows that solar wind magnetic field fluctuations have more energy than velocity fluctuations, with normalized residual energies on the order of ~ -0.5. These results are consistent with previous observations of the solar wind. They provide additional information for the characterization and modeling of the occurrence of Alfvén waves with heliocentric distance, latitude, solar cycle, and solar wind properties (Bruno and Carbone, 2013; Bavassano et al., 1998; Breech et al., 2005; Tu and Marsch, 1991).

Interestingly, σ_C was found to decrease in the quasi-parallel foreshock, possibly associated with effects from nonlinear compressive waves present in this region (see the top and middle row panels, Figure 13 in Halekas et al., 2017). On the other hand, the Alfvén ratio was found to increase as the solar wind approaches the Martian bow shock, as shown in Figure 3, making use of cylindrical Mars Solar Electric (MSE) coordinates. The MSE coordinate system is centered at Mars and its axes are defined as follows. The X-axis point towards the Sun, including correction for solar wind aberration due to Mars' orbital motion, and the Z-axis point along the convective electric field seen in the planet's rest frame ($\mathbf{E}_{SW} = -\mathbf{U}_{SW} \times \mathbf{B}_{SW}$), where $\mathbf{U}_{SW}$ and $\mathbf{B}_{SW}$ are the solar wind velocity and IMF, respectively. The Y-axis completes the right-handed system. These observations constitute another example of Mars affecting the solar wind, even upstream from the bow shock. The computed Alfvén ratio increase, from ~ 0.2 to ~ 1, is similar for both the quasi-parallel and quasi-perpendicular bow shock regions (not shown), suggesting it is likely

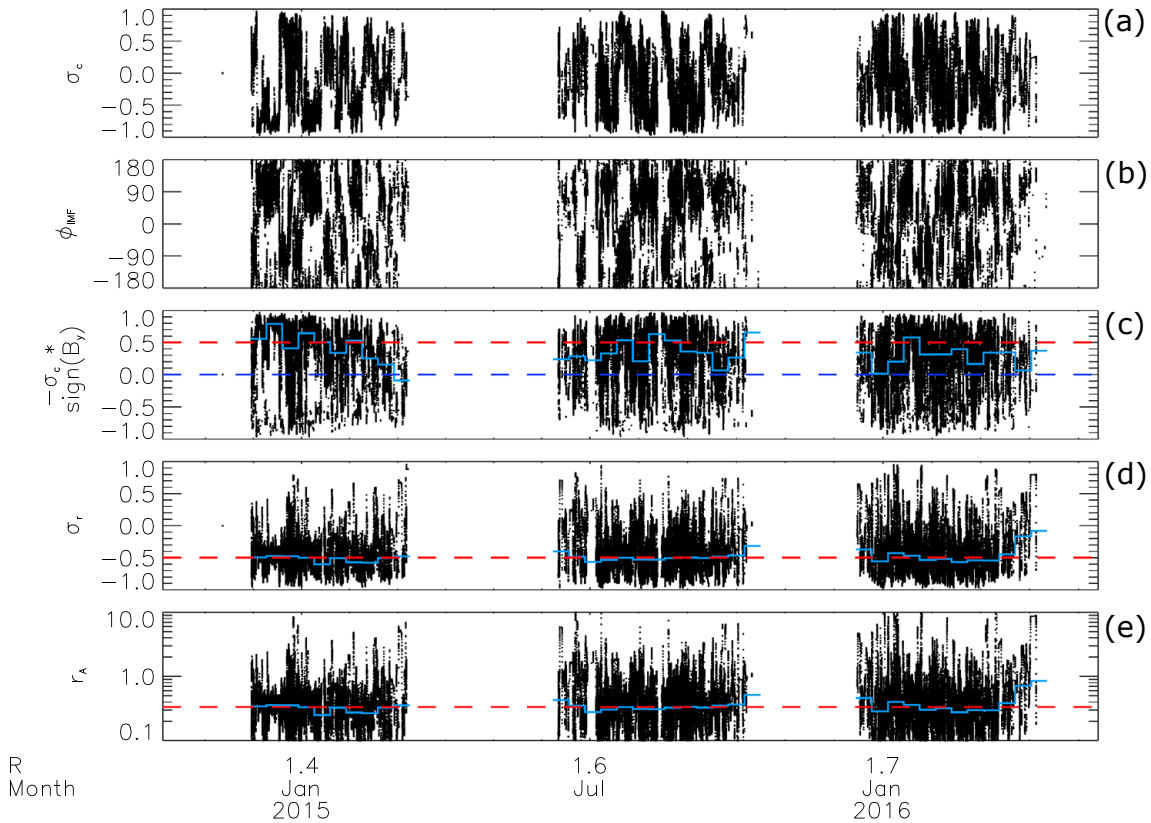

Figure 2: Solar wind properties computed from 30-minute time intervals upstream of Mars' bow shock as a function of time, between October 2014 and May 2016 (black points). (a) The normalized cross helicity (σ_C), (b) azimuthal angle of the IMF in the X-Y MSO plane $\phi_{IMF} = tan^{-1}(By/Bx)$, (c) $-\sigma_C$ multiplied by the sign of the IMF dawn-dusk (By) MSO component, (d) normalized residual energy (σ_r), (e) and Alfvén ratio (r_A). The light blue lines in panels (c-e) show the corresponding median values over 10-day intervals. The dashed red lines display the corresponding median values from March to May 2014 (MAVEN's cruise phase) for comparison. Note the dashed blue line in panel (c) is equal to zero and is shown for reference. Text labels indicate Mars's heliocentric distance (R) in astronomical units. MSO: Mars Solar Orbital. IMF: Interplanetary Magnetic Field. Source: Taken from Halekas et al. (2017).

not due to foreshock effects. As discussed in Halekas et al. (2017), the observed energy transfer from magnetic to kinetic fluctuations could be associated with solar wind mass loading by planetary pick-up ions, especially protons resulting from Mars's extended H exosphere (Halekas, 2017; Yamauchi et al., 2015; Rahmati et al., 2017).

Mass-loading is only one of several macroscopic effects associated with cumulative planetary ion pick-up. Analogous to comet pick-up ion physics, the newly ionized planetary proton population represents an additional, non-thermal component, of the total proton velocity distribution function (e.g., Mazelle et al., 2004; Gary, 1993; Delva et al., 2011; Delva et al., 2015). This distribution is capable of generating electromagnetic plasma waves upstream from the Martian bow shock, in association with different plasma instabilities (Gary, 1993). These waves affect the pristine solar wind before it encounters the bow shock and can be transmitted into the

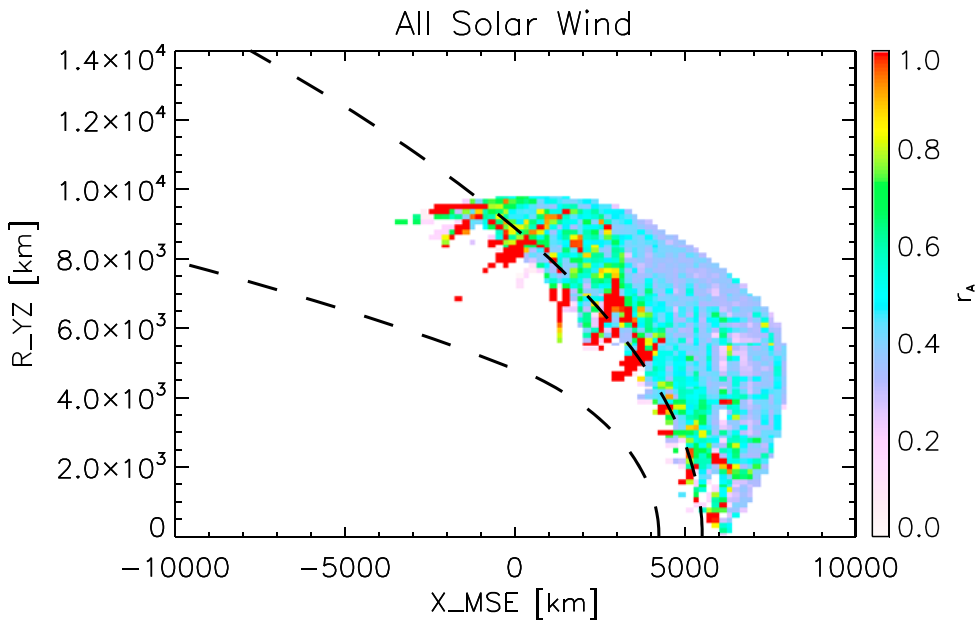

Figure 3: The normalized Alfvén ratio for solar wind measurements between October 2014 and May 2016, in cylindrical MSE coordinates. The dashed black curves display the bow shock and magnetic pile-up fits from Trotignon et al. (2006). MSE: Mars Solar Electric. Source: Taken from Halekas et al. (2017).

magnetosheath, having also effects over processes in the Martian magnetosphere (Romeo et al., 2021; Andrés et al., 2020; Romanelli et al., 2022; Ruhunusiri et al., 2017, 2015; Jiang et al., 2023).

Several parameters determine which plasma instability has the largest linear wave growth rate. Among them is the IMF cone angle, i.e., the angle between the IMF and the solar wind velocity at the time of pick-up. As shown in Brinca and Tsurutani (1989), the ion-ion right-hand resonant (RH) instability is predominant when the IMF cone angle is smaller or equal to 75°. The ion-ion left-hand resonant instability (LH) is the most unstable for IMF cone angles larger than $\sim 75°$ (Brinca and Tsurutani, 1989). Both ion-ion resonant instabilities have maximum linear wave growth rates for propagation parallel to the background magnetic field (Brinca, 1991; Gary, 1993). Therefore, the presence of pick-up ions is also responsible for the generation of ultra-low frequency waves, which, in the Hall-MHD formalism correspond to the fast magnetosonic (right-hand polarization) and the ion cyclotron waves (left-hand polarization), respectively. Such wave modes tend, in turn, to the MHD fast magnetosonic and the Alfvén linearly polarized wave modes for very low frequencies, under parallel propagation conditions (Cramer, 2001). Interestingly, the Doppler shift is responsible for the observation of these waves (RH and LH) at a frequency near the local proton cyclotron frequency in the spacecraft frame, with a left-handed elliptical polarization (Gary et al., 1989; Brinca, 1991; Gary, 1993). It is because of this

particular property that these waves are sometimes referred to as proton cyclotron waves (or PCW). However, as mentioned before, only under very specific conditions PCW do they actually correspond to the ion cyclotron (Alfvénic) wave branch. Note that the nomenclature PCW, is based on wave properties seen in the spacecraft reference frame, while the ion cyclotron wave mode is defined in the plasma rest frame.

The first report of PCW upstream from Mars' bow shock was made by Russell et al. (1990). These ultra-low frequency waves have also been detected and analyzed in greater detail thanks to magnetic field observations provided by MGS and MAVEN missions (Brain et al., 2002; Mazelle et al., 2004; Bertucci et al., 2013; Romanelli et al., 2013, 2016; Liu et al., 2020; Wei and Russell, 2006; Wei et al., 2011, 2014; Romeo et al., 2021). These waves were consistently found left-handed elliptically polarized in the spacecraft reference frame and propagating quasi-parallel to the mean IMF (with propagation angles on the order of 20°), which has been associated with nonlinear effects (e.g., Romanelli et al., 2013).

MGS and MAVEN allowed the identification of a long-term trend, with higher PCW occurrence rate near the Martian perihelion (Romanelli et al., 2013; Bertucci et al., 2013; Romanelli et al., 2016; Romeo et al., 2021). Such an annual trend is likely associated with seasonal changes in the exospheric hydrogen density and resulting newborn planetary proton density (Rahmati et al., 2017, 2018; Halekas, 2017; Yamauchi et al., 2015). Figure 4 shows the PCW occurrence rate as a function of time, as seen by MAVEN between October 2014 and February 2020. Romeo et al. (2021) reported that this rate displays an increase up to $\sim 30 - 35\%$ near (slightly after) the Martian perihelion and southern summer solstice. These values are an order of magnitude larger than the average value near the Martian aphelion ($\sim 2\%$), in agreement with previous studies (Romanelli et al., 2013; Bertucci et al., 2013; Romanelli et al., 2016). It is also worth noticing that the PCW occurrence rate increase takes place during part of the Martian dust storm season, marked by gray regions in Figure 4b (Romeo et al., 2021). In this context, Chaffin et al. (2021) reported that a regional dust storm observed well after the perihelion increased planetary H escape by a factor of five to ten, suggesting that dust dynamics affect exospheric H densities more than seasonal variations.

Recent studies have focused on the effects that PCW have on Alfvénic turbulence in the pristine solar wind (Ruhunusiri et al., 2017; Andrés et al., 2020; Romanelli et al., 2022). In particular, Andrés et al. (2020) analyzed four months of MAVEN magnetic field and plasma data, to determine if the magnetic field power spectra and/or the energy cascade rates are affected by

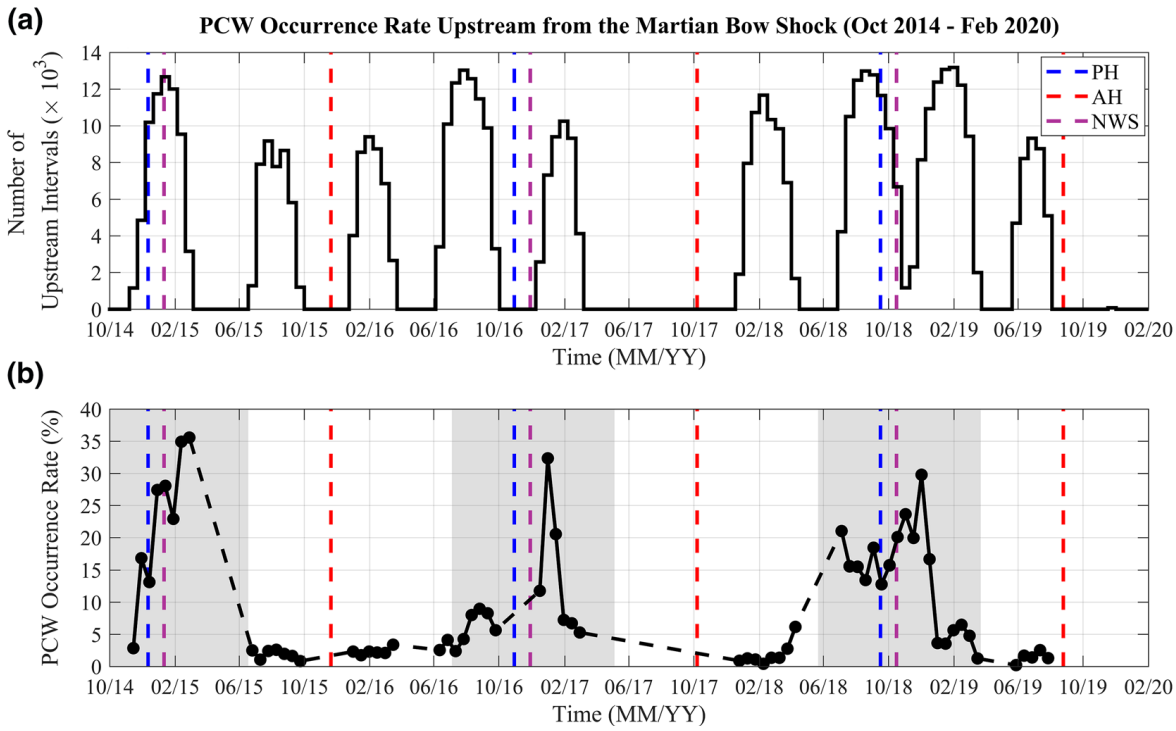

Figure 4: (a) Histogram of the number of analyzed 512 s time intervals ($\times 10^3$) upstream from Mars's bow shock as a function of time (15-day bins), between October 2014 and February 2020. (b) Derived PCW occurrence rate (%) as a function of time. The dashed black line is associated with data gaps in the upstream region (see upper panel). Gray-shaded areas correspond to periods of dust storm seasonal activity. (a-b) The blue, purple, and red vertical dashed lines correspond to the Martian perihelion (PH), the northern winter solstice (NWS), and the aphelion (AH), respectively. PCW: Proton Cyclotron Waves. Source: Romeo et al. (2021)/ John Wiley & Sons.

PCW. Figure 5 displays the magnetic field power spectral density (PSD) associated with 30-minute intervals in the pristine solar wind (Gruesbeck et al., 2018) when the IMF cone angle was approximately constant. All these events (sets A and B) have a normalized fluctuation plasma density smaller than 20%, thus corresponding to nearly incompressible solar wind conditions. Set A contains cases with PCW, while these waves are absent in the events contained in Set B (Andrés et al., 2020). As can be seen, Figure 5, left panel, shows a clear peak in the PSD at the local proton cyclotron frequency for all events. These results also show a power law decay consistent with a Kolmogorov spectrum. Indeed, wave power can be modeled as $P \propto P_0\, f^{-\gamma}$, where f is the frequency and the spectral index, $\gamma = -5/3$, is constant in the MHD scales for all cases in both sets. The observed decay is consistent with Alfvénic turbulence and does not appear to be affected by PCW at the MHD scales (Andrés et al., 2020).

Andrés et al. (2020) also estimated, for the first time, the absolute value of the incompressible energy cascade rate of the solar wind upstream from Mars bow shock at MHD scales. For this, the authors made use of the exact relation for incompressible MHD turbulence (see, e.g.,

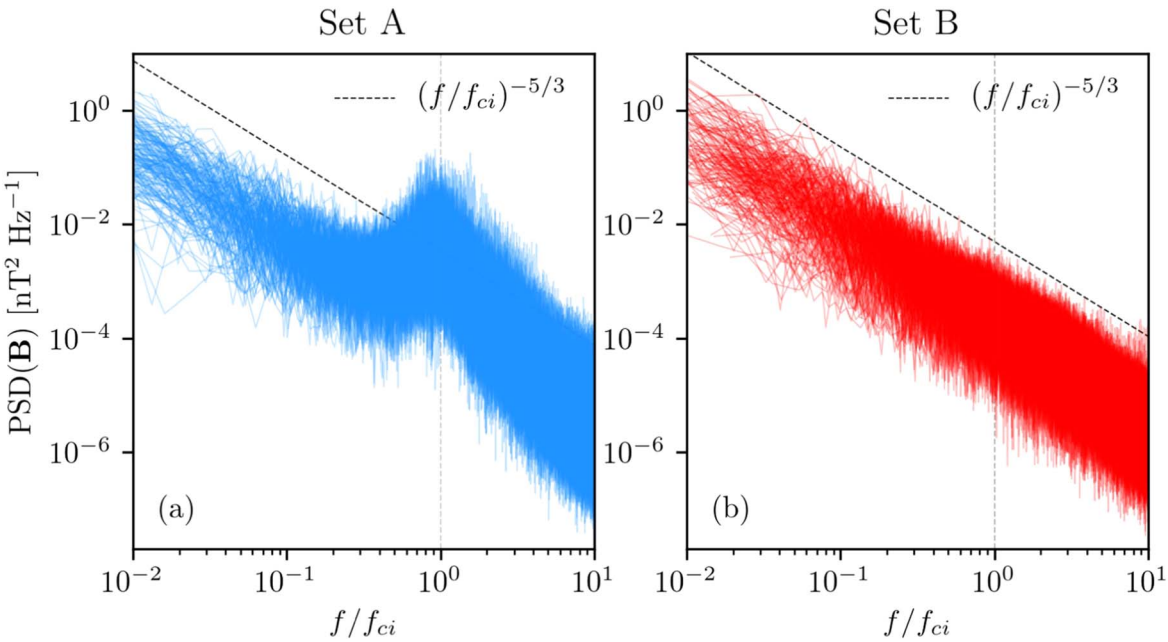

Figure 5: Magnetic field power spectra density as a function of the observed normalized frequency for 30-minute events, seen by MAVEN MAG when is upstream and magnetically disconnected from the bow shock of Mars. Set A (left) and Set B (right) consists of 184 events with PCW and 208 events without PCW, respectively. MAVEN: Mars Atmosphere and Volatile EvolutioN. MAG: Magnetometer. PCW: Proton Cyclotron Waves. Source: Taken from Andrés et al. (2020).

Politano and Pouquet, 1998a,b; Andrés et al., 2016; Ferrand et al., 2021). Since MAVEN is a single spacecraft mission, Andrés et al. (2020) assumed full isotropy and made use of the Taylor hypothesis to integrate Equation 4 in their work and compute the energy cascade rate per unit volume, ε (see, also, Stawarz et al., 2011). Under these conditions, the isotropic nonlinear energy cascade rate can be expressed as a function of time lags τ as:

$$\varepsilon = \rho_0 \langle [(\Delta\mathbf{u}\cdot\Delta\mathbf{u} + \Delta\mathbf{u}_A\cdot\Delta\mathbf{u}_A)\Delta u_\ell - (\Delta\mathbf{u}\cdot\Delta\mathbf{u}_A + \Delta\mathbf{u}_A\cdot\Delta\mathbf{u})\Delta u_{A\ell}]/(-4\tau U_0/3)\rangle. \quad (4)$$

where $u_\ell = \mathbf{u}\cdot\hat{\mathbf{U}}_0$, $u_{A\ell} = \mathbf{u}_A\cdot\hat{\mathbf{U}}_0$, and U_0 is the mean plasma flow speed. The angular bracket $\langle\cdot\rangle$ denotes an ensemble average (Pope, 2001), which was taken as the time average assuming ergodicity. Note that Equation 4 makes use of the increments definition, $\Delta\alpha \equiv \alpha' - \alpha$, where fields are evaluated at position $\mathbf{x}$ or $\mathbf{x}' = \mathbf{x} + \boldsymbol{\ell}$. A prime is added to the corresponding field in the latter case. Equation 4 shows that under the considered assumptions, ε is fully defined by velocity and magnetic field time increments, that Andrés et al. (2020) computed based on MAVEN MAG and SWIA data.

Andrés et al. (2020) reported an increase in the absolute value of the nonlinear solar wind incompressible energy cascade rate at MHD scales ($\langle|\varepsilon|\rangle_{MHD}$), when PCW are detected in the

pristine solar wind. However, the known variability of PCW with the Martian heliocentric distance and the relatively small data set analyzed prevented the authors from determining the factor(s) responsible for such an increase. Making use of more than five years of MAVEN measurements and a similar methodology, Romanelli et al. (2022) concluded that $\langle|\varepsilon|\rangle_{MHD}$ displays a decreasing trend with the Martian heliocentric distance, in agreement with other studies (e.g., Hadid et al., 2017; Bandyopadhyay et al., 2020; Andrés et al., 2021). Moreover, the presented results suggest that PCW do not have a significant effect on $\langle|\varepsilon|\rangle_{MHD}$ (Romanelli et al., 2022). Figure 6a shows that the probability distribution function of log $\langle|\varepsilon|\rangle_{MHD}$ for conditions associated with Martian perihelion does not change significantly due to the presence of PCW. Both distributions are similar with log $\langle|\varepsilon|\rangle_{MHD}$ values ranging from ~ -19 to ~ -15, with $\langle|\varepsilon|\rangle_{MHD}$ median values equal to 1.4×10^{-17} J m^{-3} s^{-1} and 1.5×10^{-17} J m^{-3} s^{-1}, for cases at perihelion with and without PCW, respectively. In contrast, Figure 6b displays a clear shift of the distribution with larger $\langle|\varepsilon|\rangle_{MHD}$ values around the Martian perihelion. The $\langle|\varepsilon|\rangle_{MHD}$ median value is equal to 1.5×10^{-17} J m^{-3} s^{-1} and 4.6×10^{-18} J m^{-3} s^{-1}, for perihelion and aphelion conditions, respectively (Romanelli et al., 2022).

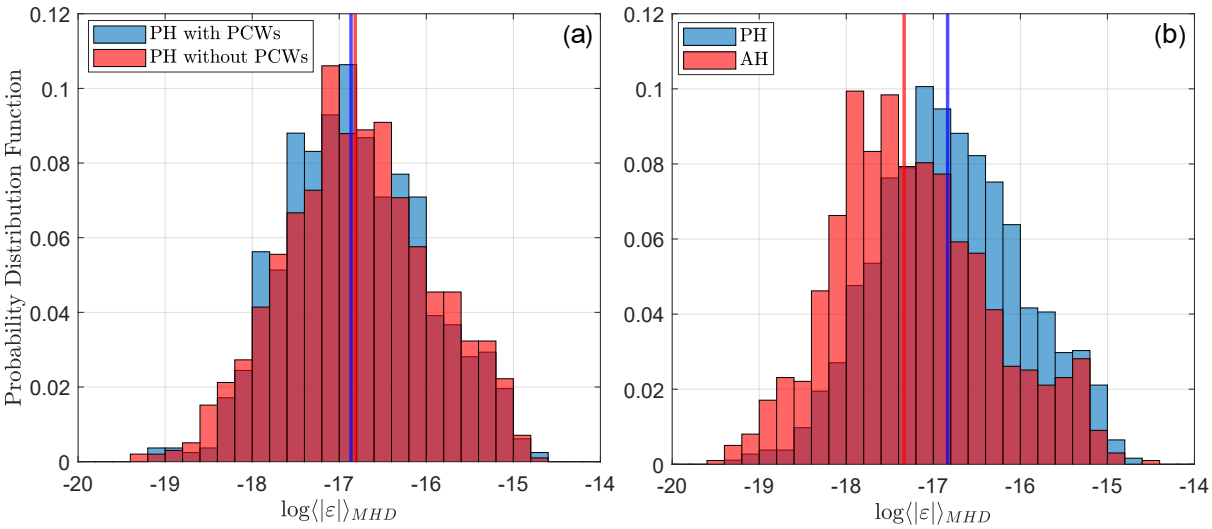

Figure 6: Probability distribution function of $\log\langle|\varepsilon|\rangle_{MHD}$ for different Martian orbital locations and PCW activity. (a) Martian perihelion with PCW (blue) and without PCW (red) (b) Martian perihelion conditions (with and without PCW, blue) and aphelion conditions (with and without PCW, red). (a-b) The vertical solid lines correspond to the median of the respective distributions. PCW: Proton Cyclotron Waves. Source: Taken from Romanelli et al. (2022)/ IOP Publishing/CC BY 4.0.

It is worth noticing that these results do not rule out the possibility of PCW effects on Alfvénic turbulence at kinetic scales. Complementary studies are needed to potentially identify these effects, using plasma observations with a higher sampling frequency and theoretical models of solar wind turbulence in this regime (Galtier, 2008; Andrés et al., 2018). Moreover, future

studies could also focus on the effects that planetary foreshocks and associated wave activity have on solar wind turbulence. Planetary foreshocks are filled with electromagnetic plasma waves in different frequency ranges and can affect the nonlinear energy cascade rate in the MHD and kinetic scales (Eastwood et al., 2005; Burgess et al., 2012). The variability of solar wind properties and IMF strength and direction with heliocentric distance also offers the possibility to perform comparative analyses (e.g., Andrés et al., 2015; Meziane et al., 2017; Romanelli et al., 2018a, 2020a; Romanelli and DiBraccio, 2021; Jarvinen et al., 2022; Glass et al., 2023). In this regard, numerical simulations also constitute a particularly useful approach to understand better these environments, improve data interpretation, and point towards fundamental physical processes taking place (e.g., Jarvinen et al., 2022).

3 Alfvén waves in the Martian magnetosheath

Identifying wave modes in planetary magnetosheaths is particularly challenging for several reasons. Waves in the magnetosheath can be generated upstream and convected by the solar wind, can be generated at the bow shock, and/or be associated with local plasma instabilities (e.g., Dubinin and Fraenz, 2016; Harada et al., 2019). In the case of Mars, the latter also includes effects derived from the presence of planetary protons and oxygen ions (e.g., Chaffin et al., 2015; Clarke et al., 2017; Deighan et al., 2015; Feldman et al., 2011; Halekas, 2017; Barabash et al., 1991; Curry et al., 2015; Rahmati et al., 2015, 2017; Yamauchi et al., 2015; Dong et al., 2015). Furthermore, normal wave modes can be coupled in a nonuniform medium such as the magnetosheath (Cramer, 2001).

It is also important to remark that conditions in the magnetosheath present asymmetries related to the local IMF and due to the deflection of the solar wind around Mars (Dubinin et al., 2018; Romanelli et al., 2020b). The former gives rise to temperature anisotropies, particularly downstream of the quasi-perpendicular bow shock (Espley et al., 2004; Halekas et al., 2020; Simon-Wedlund et al., 2022a; Jin et al., 2022; Simon-Wedlund et al., 2022b). The latter is responsible, for example, for superAlfvénic conditions in the Martian magnetosheath flanks, while the shocked solar wind is significantly decelerated near the subsolar MPB (Halekas et al., 2020).

A detailed study on the electromagnetic wave power spatial distribution around Mars at different frequency ranges has been reported by Fowler et al. (2017). The magnetosheath was found to be

the region with the strongest magnetic field wave power in the ULF range (Dubinin and Fraenz, 2016; Fowler et al., 2017). This is associated with processes contributing to dissipating the bulk kinetic energy of the pristine solar wind (e.g., Papadopoulos, 1971; Auer et al., 1971; Burgess et al., 1989). Figure 7 left (right) column displays the magnetic field power distribution in the $X_{MSE} - Z_{MSE}$ ($X_{MSE} - Y_{MSE}$) plane.

Figures 7a and 7b show that most of the magnetic field wave power for frequencies between 0.01 Hz and 0.05 Hz lies in the magnetosheath, upstream of the terminator plane. Magnetic field wave power is also significant in the magnetotail, although it is approximately one order of magnitude weaker throughout this region. The absence of a significant decrease in magnetic field ULF wave power between the magnetosheath and the ionosphere, shown in Figures 7a and 7b, is consistent with the expected lack of complete ion thermalization in the magnetosheath. Indeed, the relatively small size of the Martian magnetosheath (its thickness along the Mars-Sun axis is $\sim$ 1200 km) compared to ion spatial scales (e.g., the convected solar wind proton gyroradius is $\sim$ 1000 km) implies that kinetic effects are relevant and suggests that thermalization is likely incomplete before plasma reaches the MPB and inner regions of the Martian magnetosphere (Moses et al., 1988; Kallio et al., 2011; Ruhunusiri et al., 2017; Jiang et al., 2023). Thermalization processes involve space and time scales related to local ion gyrofrequencies, which in the Martian magnetosheath are near the ULF range (Fowler et al., 2017).

Figures 7c and 7d show that magnetic wave power in the 1-5 Hz range is maximum near the subsolar region and along the Martian bow shock. Wave power takes smaller values in the Martian magnetosheath and is three orders of magnitude smaller in the tail. Figures 7e and 7f show that wave power at 5 Hz presents a similar spatial distribution to that of between 1-5 Hz, but is two orders of magnitude smaller. Local maxima in the wave power at magnetospheric boundaries make evident that the solar wind kinetic energy is transferred to particle heating in these very thin regions. Moreover, the associated particle velocity distribution function has potentially sufficient free energy for the local generation of electromagnetic waves. Magnetic field wave power is also significant slightly upstream of the average bow shock location. This is due to several factors: the non-stationarity of this boundary, the presence of reflected ions at the shock, over and undershoots, and electromagnetic plasma waves. Among the latter, whistler waves, likely generated at the shock, are capable of propagating into and affecting the upstream region (Trotignon et al., 2006; Halekas, 2017; Edberg et al., 2009a,b; Paschmann et al., 1981; Gosling et al., 1982; Eastwood et al., 2005; Mazelle et al., 2004; Livesey et al., 1982).

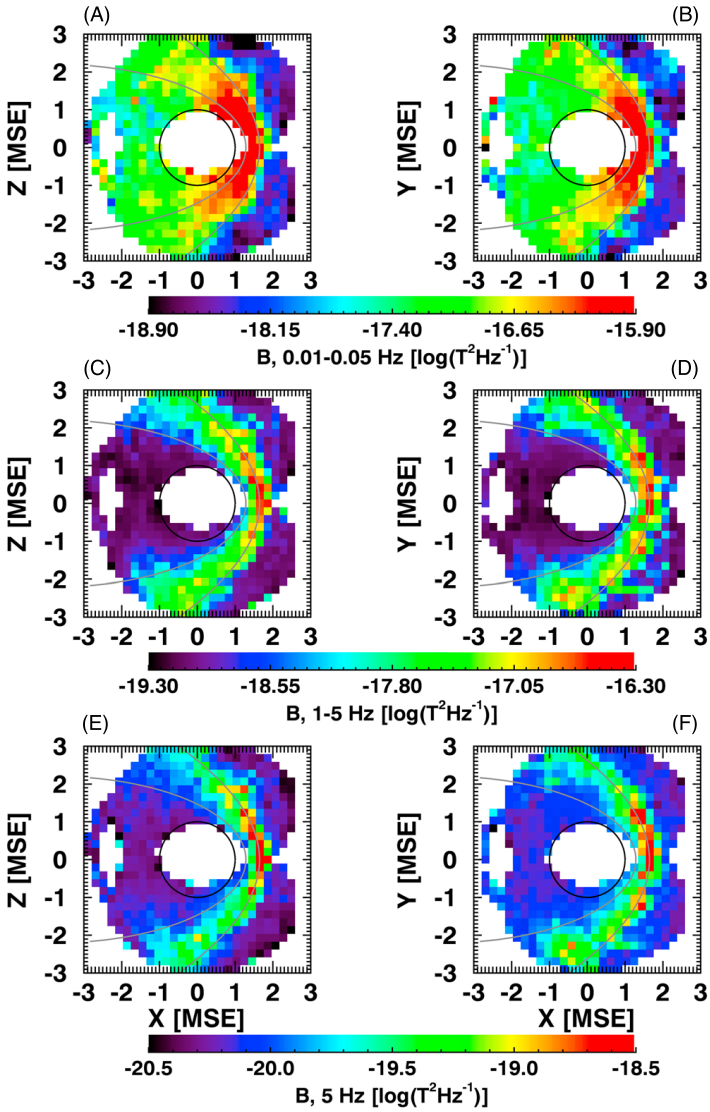

Figure 7: Statistical magnetic field strength wave power for several frequency ranges, for altitudes greater than 600 km. (a and b) 0.01–0.05 Hz, (c and d) 1–5 Hz, and (e and f) 5 Hz. The left and right columns correspond to projections onto the X-Z and X-Y MSE planes, respectively. MSE: Mars Solar Electric. Source: Fowler et al. (2017)/ John Wiley & Sons.

So far, the identification of wave modes in the Martian magnetosheath has been performed by computing transport ratios, interpreted in terms of MHD linear theory. Following the method firstly developed by Gary (1993) and extended by Song et al. (1994), Ruhunusiri et al. (2015) identified low-frequency wave modes as Alfvén and quasi-parallel slow waves (indistinguishable by the employed methodology), fast, quasi-perpendicular slow, and mirror mode waves. This was done based on four transport ratios: the transverse ratio (T_R), the compressional ratio (C_R), the phase ratio (P_R) and the Doppler ratio (D_R). These are defined in terms of velocity, magnetic field, and density fluctuations as follows:

$$T_R = \frac{\delta\mathbf{B}\cdot\delta\mathbf{B} - \delta B_{\parallel}^2}{\delta B_{\parallel}^2} \tag{5}$$

$$C_R = \frac{\delta n_i^2}{n_{i0}^2} / \frac{\delta\mathbf{B}\cdot\delta\mathbf{B}}{B_0^2} \tag{6}$$

$$P_R = \frac{\delta n_i}{n_{i0}} / \frac{\delta B_{\parallel}}{B_0} \tag{7}$$

$$D_R = \frac{\delta\mathbf{u}_i\cdot\delta\mathbf{u}_i}{u_{i0}^2} / \frac{\delta\mathbf{B}\cdot\delta\mathbf{B}}{B_0^2} \tag{8}$$

where $\delta B_{\parallel}$ is the component of the magnetic field fluctuation ($\delta\mathbf{B}$) parallel to the background magnetic field $\mathbf{B_0}$. In addition, δn_i, n_{i0}, $\delta\mathbf{u}_i$, and u_{i0} are the ion number density fluctuation, mean value, the fluctuation in the velocity field, and the mean ion velocity, respectively. The wave mode identification method developed by Song et al. (1994) assumes that a single wave mode is dominant at a single frequency with a single wavenumber. In addition, it is applicable in a high beta plasma, suggesting the results reported by Ruhunusiri et al. (2015) are most accurate in the Martian magnetosheath. Table 1 in Ruhunusiri et al. (2015) reports the range of values for the transport ratios (Equations 5-8) used to identify low-frequency wave modes in the Martian magnetosphere.

Figure 8 displays maps of the wave mode occurrence ratio, based on MAVEN MAG, SWIA and Suprathermal and Thermal Ion Composition (STATIC) (McFadden et al., 2015) data between 7 October 2014 and 28 April 2015, in cylindrical MSO coordinates. Ruhunusiri et al. (2015) found a very high wave occurrence rate of Alfvén and quasi-parallel slow waves in the pristine solar wind and the magnetosheath (panel a). Several of the wave events upstream from the bow shock are likely Alfvén waves, in agreement with previous studies of upstream ULF waves and solar wind turbulence (e.g., Andrés et al., 2020; Halekas et al., 2020). Moreover, the observed occurrence rate decrease from the upstream region into the magnetosheath may be indicative of upstream Alfvén wave convection. Ruhunusiri et al. (2015) also reported a significant amount of fast magnetosonic waves in the Martian magnetosheath that increases closer to the MPB (panel b). The source of these magnetosonic waves could be mode conversion at the bow shock or PCW and foreshock wave transmission from upstream to the magnetosheath. In addition, the authors also concluded there is a minor mirror mode wave population that is observed more frequently near the dayside magnetosheath region (panel d), in agreement with other magnetic field observations (Espley et al., 2004; Simon-Wedlund et al., 2022a,b). Given that the wave identification method by Song et al. (1994) may not be applied downstream of the MPB (low

beta plasma region) the authors did not provide final conclusions about waves in this region (Ruhunusiri et al., 2015).

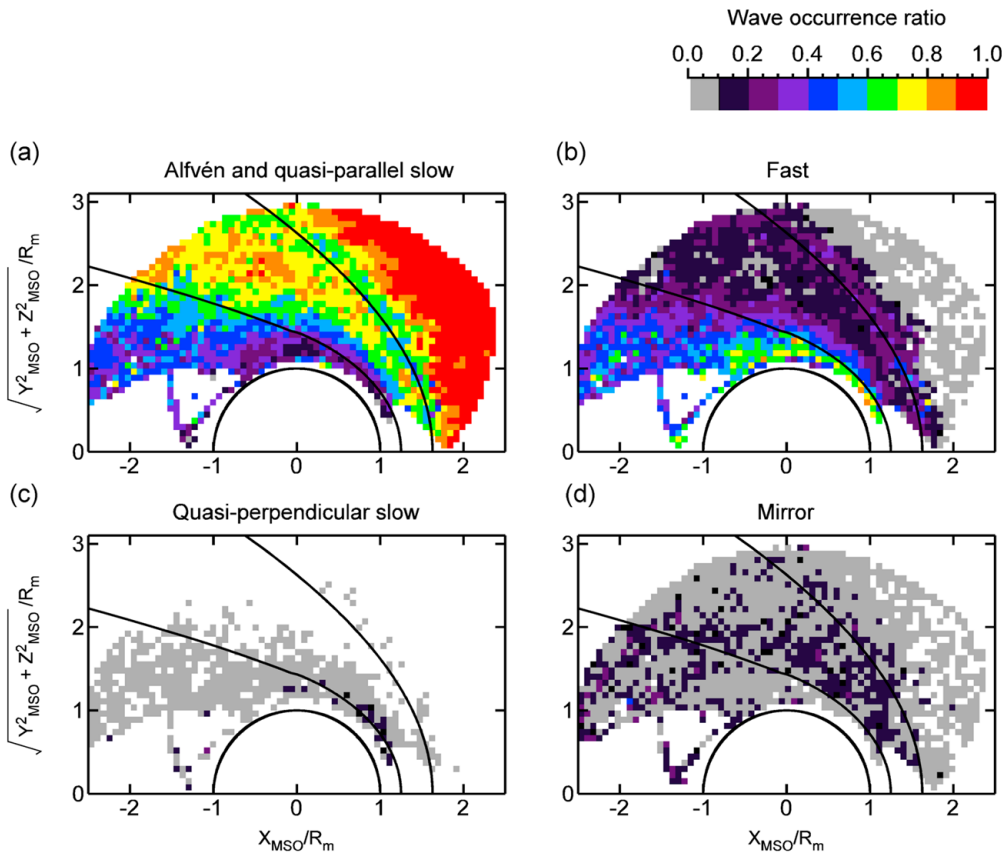

Figure 8: Occurrence rate of several low-frequency wave modes. (a) Alfvén and quasi-parallel slow, (b) fast magnetosonic, (c) quasi-perpendicular slow, (d) mirror. Taken from Ruhunusiri et al. (2015) based on the identification technique developed in Song et al. (1994) for high beta plasmas.

The previous analysis was not concerned with the nonlinear interaction between fluctuations of different temporal and spatial scales. Ruhunusiri et al. (2017) performed the first global characterization of turbulence in the Martian magnetosphere, based on the computation of spectral indices for perturbations observed in the magnetic field. As mentioned before, these indices are the slopes associated with the magnetic field power spectra distribution as a function of the observed frequency (in logarithmic scale). They provide information about the physical processes at play within a given frequency range (energy injection, transfer or cascade, and dissipation). In contrast with observations in the pristine solar wind, Ruhunusiri et al. (2017) concluded there is not an inertial range in the Martian magnetosheath following Kolmogorov's scaling (where $\gamma = -5/3$) expected when energy is transferred between scales.

Figure 9 shows the median magnetic field power spectral density as a function of the normalized frequency for several Martian solar longitude (L_s) values. L_s is the angle between Mars and

the Sun, measured from the northern hemisphere spring equinox where $L_s = 0°$. The Martian perihelion and aphelion correspond to $L_s = 251°$ and $L_s = 71°$, respectively. The northern hemisphere summer (winter) solstice occurs at $L_s = 90°$ ($L_s = 270°$). Ruhunusiri et al. (2017) found that the spectral indices in the magnetosheath (panel b) take larger values ($\gamma \sim -0.5$) for frequencies smaller than the local proton gyrofrequency and much more negative values ($\gamma \sim -2.7$) at higher frequencies. This is in agreement with observations at other planetary magnetosheaths and suggests that the shocked solar wind, heated and slowed down at the bow shock, is composed of fluctuations that do not have sufficient time to interact nonlinearly and give rise to a fully developed energy cascade rate (e.g., Hadid et al., 2015; Zimbardo et al., 2010; Tao et al., 2015). Although there seem to be some effects of PCW in the Martian magnetosheath spectra, they do not appear as pronounced as in the region upstream of the bow shock (panel a). Note the clear peak at $f/f_{H^+} \sim 1$, for $L_s \sim 270°$ when MAVEN is in the upstream region. In other words, the Martian magnetosheath appears to be filled with high amplitude Alfvén waves that have not reached a fully developed turbulent regime, at least near the terminator plane (Ruhunusiri et al., 2015, 2017; Fowler et al., 2017).

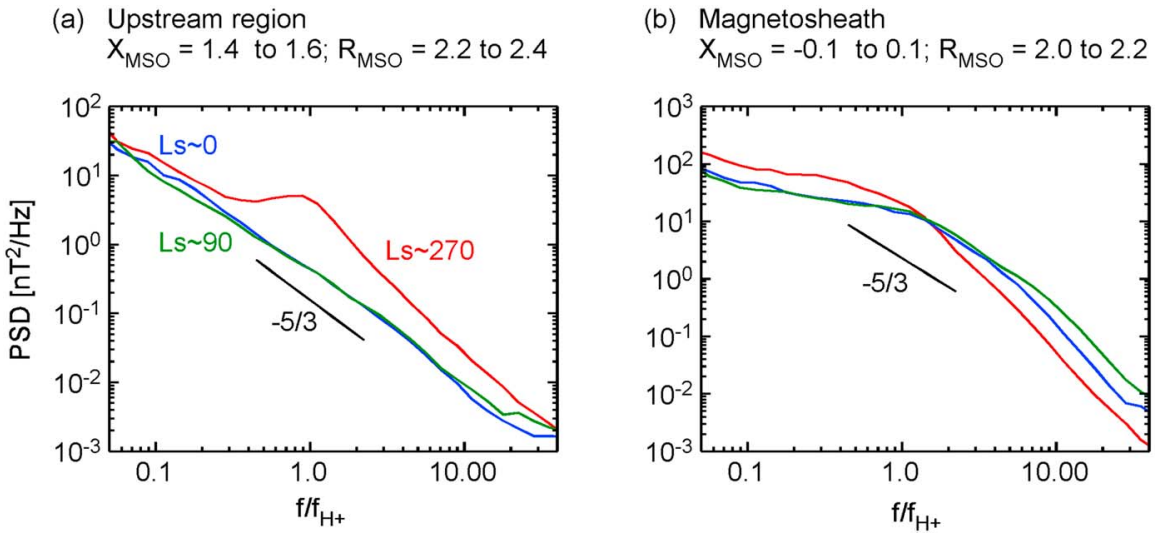

Figure 9: Median magnetic field power spectra density as a function of the normalized frequency for three seasons in (a) the region upstream of the Martian bow shock and (b) the Martian magnetosheath. f_{H^+} refers to the local proton cyclotron frequency. L_s is the Martian solar longitude. Source: Ruhunusiri et al. (2017)/ John Wiley & Sons.

Similar conclusions have also been reached by Jiang et al. (2023). However, the authors also reported the presence of a Kolmogorov-like spectrum in the Martian magnetosheath for very low wave frequencies. The authors found magnetic field spectra in the Martian magnetosheath consisting of triple power laws, where the intermediate regime displays a plateau. An example of such events is shown in Figure 10. Note that their breaking frequency points are typically

between $\sim 10^{-2}$ to $\sim 10^{-1}$ and ~ 1 to ~ 10 times the local gyrofrequency, respectively, depending on different parameters, such as the plasma beta (see Figure 7c and 7d in that work). Their statistical analysis allows the identification of a significant correlation between the occurrence rate of plateau power spectra and planetary proton pick-up ion parameters. Specifically, the authors suggest the formation of plateau-like spectra may be due to energy injection associated with PCW (Jiang et al., 2023). It is possible, however, that a fully developed energy cascade rate is reached further downstream from the planet, along the magnetosheath flanks. Future studies may shed light on this matter.

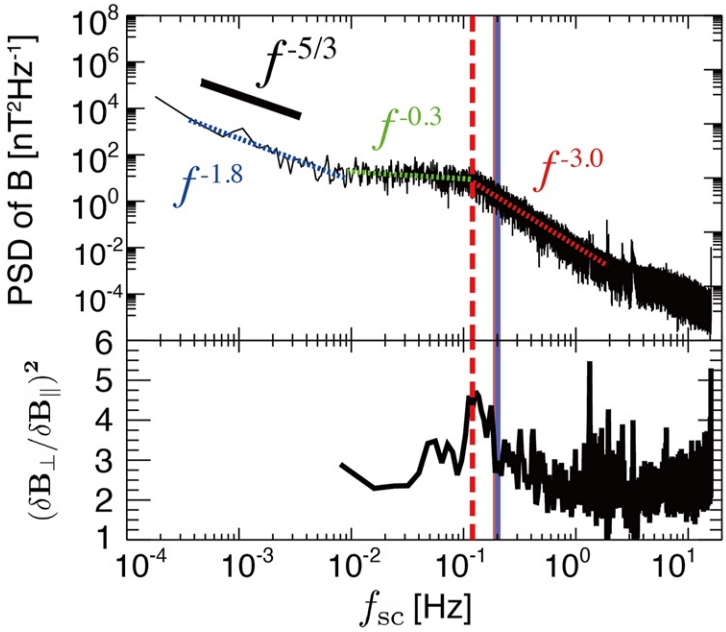

Figure 10: (Upper) Magnetic field power spectral density for a Martian magnetosheath interval on 4 June 2016, between 21:10 UT and 22:43 UT. Vertical lines correspond to relevant ion-scale frequencies. The red dashed line shows the highest frequency breakpoint f_{bk2}= 0.12 Hz. The light red and light blue lines display $f_{\rho i}$ and f_{di}, respectively, with $f_{\rho i} = V_i/2\pi\rho_i$, $f_{di} = V_i/2\pi d_i$, where V_i is the local plasma bulk velocity, ρ_i is the local thermal proton gyro-radius, and d_i is the proton inertial length. (Lower) Square of the magnetic field perpendicular fluctuation normalized by the magnetic field parallel fluctuation, as a function of the observed frequency in the spacecraft reference frame. Source: Jiang et al. (2023) / John Wiley & Sons.

4 Alfvén waves inside the MPB and the ionosphere

While there have been studies of Alfvén waves in several regions of the Martian magnetosphere, there are far fewer studies focused on this phenomenon within the Martian MPB and ionosphere. This is likely due to a combination of factors such as a relatively low level of wave activity and the lack of adequate instrumentation and spacecraft sampling until more recent missions.

Figure 11 shows the compressional ratio C_R is larger than 1 inside the Martian MPB. This result is observed both using MAVEN SWIA (panel a) and STATIC (panel b) data and suggests Alfvén waves are not commonly present in the magnetic pile-up region and magnetotail (Ruhunusiri et al., 2015). In addition, as can be seen in Figure 7, the magnetic field wave power decreases downstream of the MPB, particularly in the magnetotail. This could be due to relatively weak energy dissipation processes in the explored frequency ranges, as well as the much lower plasma beta values in this region (Fowler et al., 2017). The spectral indices in the magnetic pile-up region and the Martian wake are near -2 or smaller in both the MHD and kinetic ranges (Ruhunusiri et al., 2017). The lack of a spectral break at the local proton cyclotron frequency may result from the plasma containing primarily heavy planetary ions instead of protons (Ruhunusiri et al., 2017). Previous reports have found similar results for the Venusian wake at frequencies between 0.01 and 0.5 Hz (Vörös et al., 2008a,b).

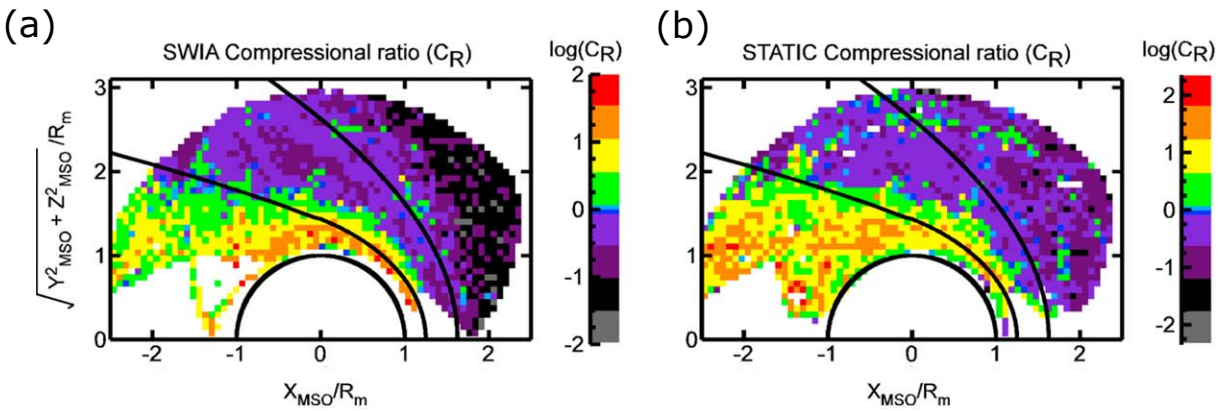

Figure 11: Compressional ratio C_R based on MAVEN MAG and SWIA (panel a) and STATIC (panel b) observations as a function of cylindrical MSO coordinates. MAVEN: Mars Atmosphere and Volatile EvolutioN. MAG: Magnetometer. SWIA: Solar Wind Ion Analyzer. STATIC: Suprathermal and Thermal Ion Composition. MSO: Mars Solar Orbital. Source: Ruhunusiri et al. (2015)/ John Wiley & Sons.

The absence of Alfvén wave observations in the Martian ionosphere and/or along crustal magnetic fields may also be the result of limited instrumentation and spacecraft orbital geometry. Early Mars orbiters, such as Phobos-2, carried magnetometers but did not sample the ionosphere. More recent missions such as MGS and MEX periodically sampled the ionosphere, but their ionospheric coverage was limited. While MGS MAG/Electron Reflectometer provided observations of the electromagnetic wave environment at Mars, the $\sim$ 400 km circular orbit precluded any comprehensive study within the ionosphere. In contrast, MEX periapsis altitudes reach down to $\sim$275 km, providing in situ samples of the topside upper Martian ionosphere but it is unable to reach the main ionospheric peak, located at $\sim$125 km altitude at the sub-solar point. Indeed, the main peak has been observed via remote sensing using the Mars Advanced

Radar for Subsurface and Ionospheric Sounding radar on MEX (e.g., Gurnett et al., 2005; Dubinin et al., 2006; Orosei et al., 2015; Picardi et al., 2004). Moreover, the lack of a magnetometer onboard MEX precludes any detailed study of the electromagnetic wave environment. In the case of MAVEN, periapsis typically lies between 150 and 200 km, determined by targeting a specific neutral density corridor. MAVEN completed nine deep dip campaigns during the first few years of its mission, where periapsis altitude was lowered to $\sim$125 km for roughly week-long periods. This enabled MAVEN to sample down to the main ionospheric peak at mid to high solar zenith angles ($\sim 45^\circ - 90^\circ$). Also, MAVEN's precessing orbit provides comprehensive coverage throughout the magnetosphere and the Martian ionosphere.

The disparity in the study of Alfvén waves within the Martian ionosphere, compared to the rich and diverse collection of work related to their analysis within the terrestrial ionosphere, also likely lies in the underlying limitations of in-situ plasma measurements made at bodies other than Earth. In spite of particle and field measurements becoming more commonplace on interplanetary missions, their sampling frequency is typically much lower than their terrestrial counterparts. For example, the ion (electron) distribution functions measured by the MEX Analyser of Space Plasma and Energetic Atoms 3 - Ion Mass Analyzer - (Electron Mass Spectrogram) are accumulated over 192 (4) seconds, and MAVEN STATIC and Solar Wind Electron Analyzer ion and electron distribution functions are accumulated over 4 and 2 seconds, respectively (Dubinin et al., 2006; McFadden et al., 2015; Mitchell et al., 2016). Such measurements typically resolve the macro-scale parameters of the system, however, they are usually limited in resolving kinetic scale physics based on electromagnetic waves at frequencies of a few Hz up to 1000s Hz in the Martian plasma environment. In contrast, terrestrial space physics missions such as Cluster, Fast Auroral SnapshoT (FAST), and Magnetospheric Multiscale (MMS) measure the ion and electron distribution functions at tens of milliseconds (Escoubet et al., 1997; Carlson et al., 1998; Burch et al., 2016). The fields measurements (i.e. magnetic and electric fields) on interplanetary missions suffer from similar limitations: magnetic field data are typically limited to DC measurements at 32 Hz (compared to AC measurements of kHz at Earth), while only a single year of 1D electric field wave power spectra is available for Mars, made by the MAVEN Langmuir Probe and Waves (LPW) instrument (Fowler et al., 2017; Andersson et al., 2015).

Recent studies have shown electromagnetic waves inside the MPB (e.g., Harada et al., 2016), in the ionosphere (e.g., Gurnett et al., 2010; Esman et al., 2022), and the Martian surface (e.g., Johnson et al., 2020; Mittelholz et al., 2021, 2023); some of them in connection with

upstream processes leading to their generation (e.g., Fowler et al., 2020; Wang et al., 2023; Shane et al., 2019; Shane and Liemohn, 2021; Shane and Liemohn, 2022). These have been primarily whistler waves observed at the interaction region between the shocked solar wind and the upper ionosphere. A comprehensive study on the occurrence rate and spatial distribution of these waves has not been undertaken yet. Next, we briefly review these works, which illustrate some of the potential effects Alfvén waves generated upstream may have in the Martian ionosphere.

Fowler et al. (2020) showed that whistler waves are produced in the upper ionosphere via a process known as 'magnetic pumping'. A summary of their event is shown in Figure 2 of their work. The free energy to drive the generation of the whistler waves is sourced from ULF compressive magnetosonic waves that are generated due to the Mars-solar wind interaction and that propagate across the draped magnetic field into the dayside ionosphere. Adiabatic compression of the plasma along wave fronts in the magnetic field acts to drive the electron distribution function unstable to the generation of whistler waves by creating an anisotropic distribution (e.g., Kennel and Petschek, 1966). The whistler waves were shown to break the reversibility of the underlying ULF magnetic pumping via efficient wave-particle interactions with the anisotropic electrons, leading to localized heating of this population. Such heating may play important roles in, for example, driving ionospheric photochemistry (Fox and Bakalian, 2001), the dissociative recombination of O_2^+ (Lillis et al., 2017), and the creation of ambipolar electric fields (-∇p_e) that can drive ions to escape to space (Ergun et al., 2016). Further study is needed to fully evaluate the impact on the energy and dynamics of the Martian ionosphere and to determine the occurrence rate of this process.

On the other hand, Wang et al. (2023) observed whistler waves within localized 'magnetic dips' at the interaction region between the solar wind and upper dayside ionosphere, in a manner postulated to be similar to whistler wave generation in the equatorial magnetosphere (e.g., LeDocq et al., 1998). The exact whistler generation mechanisms could not be determined, but temperature anisotropy and electron beam instabilities were proposed as likely candidates. The background plasma environment at Mars is such that these whistler waves propagate at much slower velocities than at Earth and so localized heating rather than propagation of the whistlers may be more important at Mars. Additional analysis is required to better understand the effects these waves have on the local plasma dynamics.

In addition, a comprehensive series of papers by Shane et al. (2019); Shane and Liemohn (2021); Shane and Liemohn (2022) used numerical approaches to demonstrate that whistler wave-particle

interactions with suprathermal electrons can explain observed pitch angle distributions (PADs) on closed crustal field lines which intersect the Martian ionosphere. Many previous studies have shown that >100 eV PADs on dayside closed field lines are isotropic or trapped, however, these PADs are not expected based on collisional scattering and conservation of adiabatic invariants alone (which are important as the electrons mirror within the closed crustal field loops) (e.g., Liemohn et al., 2003; Brain et al., 2007). Numerical calculations of the bounce-averaged electron diffusion coefficients show that wave-particle interactions are more efficient than Coulomb collisions above the exobase region and can play an important role in shaping the PADs in a manner consistent with observations (Shane and Liemohn, 2021). Numerical simulation of the bounce-averaged electron diffusion equation, including whistler wave resonance, demonstrated that such whistler wave-particle interactions alter the PADs and are consistent with observations (Shane and Liemohn, 2022). The authors noted that future work should determine whether the frequency of whistler waves is high enough to explain the average behavior in observed PADs, and determine how such whistler waves would be generated.

Several studies have also shown that solar wind pressure pulses can be convected into the bow shock and 'ring' the planetary magnetosphere (e.g., Collinson et al., 2018). Pressure pulses propagate through the magnetosphere in the form of fast magnetosonic waves (traveling across the draped magnetic field), where they can reach both the day and nightside ionosphere and drive heating of the light and heavy ion species through a variety of wave-particle interaction processes (Fowler et al., 2018b, 2021).

A final note should be made with respect to the localized crustal magnetic field regions at Mars. These regions act as 'mini-magnetospheres' that rotate with the planet, and can sporadically magnetically reconnect with the solar wind IMF (e.g., Weber et al., 2020; Bowers et al., 2023) to create 'mini cusp like' regions. Given the similarity of these cusp regions with the auroral zones at Earth, one may expect electromagnetic waves to play similar crucial roles in the physical processes present in these regions (primarily precipitation and auroral physics (Andre and Yau, 1997)). In particular, Ergun et al. (2006) performed numerical calculations to show that electromagnetic waves associated with the Mars-solar wind interaction and field-aligned currents in regions of crustal magnetic fields could heat ionospheric O^+ and O_2^+ to escape energy and drive escape rates of $\sim 10^{25}$ s^{-1}, via cyclotron damping. Their predictions closely match total ion escape rates that have been calculated based on recent observations in the magnetotail region of Mars (e.g., Dong et al., 2015; Ramstad et al., 2015; Brain et al., 2015). However, the full range

of ion energization mechanisms has not been comprehensively identified or quantified. There are still many open questions about the initial acceleration of ions in the Mars ionosphere, and the role that electromagnetic waves play in it (Hanley et al., 2022). In addition, a full 3D electric field in-situ instrumentation at low and medium frequencies, together with magnetic field and particle measurements, are needed in order to identify the exact wave modes taking place in these regions.

5 Conclusions

Over the last few years, there has been significant progress in characterizing the Alfvénic input and content of the Martian magnetosphere. The pristine solar wind, upstream of Mars's bow shock, has been characterized in terms of Alfvénic turbulence, where the absolute value of the incompressible nonlinear energy cascade rate is on the order of 10^{-17} J m^{-3} s^{-1} at MHD scales. Studies have also shown that the cascade rate varies with Mars' heliocentric distance, in agreement with investigations focused on the solar wind closer to the Sun and upstream of other planetary magnetospheres (Andrés et al., 2020; Romanelli et al., 2022; Hadid et al., 2017; Bandyopadhyay et al., 2020; Andrés et al., 2021). Moreover, values of normalized cross-helicity and residual energy show that the solar wind presents more Alfvén waves propagating outwards from the Sun (than inwards) and that the magnetic field fluctuations have more energy than the kinetic field counterpart (Andrés et al., 2020; Halekas et al., 2017). PCW associated with the extended hydrogen corona do not appear to modify the solar wind energy cascade rate at MHD scales, although their energy could have potential effects on the kinetic regime (Romanelli et al., 2022). The magnetosheath is characterized by high amplitude wave activity, and a high occurrence rate of Alfvén waves, although other wave modes are also present (Ruhunusiri et al., 2015; Fowler et al., 2017). The large amplitude waves are likely the result of (incomplete) thermalization processes of the solar wind. The relatively small size of the magnetosheath, together with potential effects from the bow shock, PCW, and other wave modes are also responsible for a magnetic field turbulent spectrum that is not fully developed (Fowler et al., 2017; Jiang et al., 2023). Among the secondary wave populations in the magnetosheath, there exists a significant component of fast magnetosonic waves and a minor contribution of mirror mode waves, particularly in the dayside (Ruhunusiri et al., 2015; Espley et al., 2004; Simon-Wedlund et al., 2022b). Downstream of the magnetic pile-up boundary, waves generally display less magnetic field power (Fowler et al., 2017). The PSD of the magnetic field does not show a Kolmogorov-like spectrum

but rather is characterized by a spectral index more negative both below and above the local proton gyrofrequency (Ruhunusiri et al., 2017).

Early studies of the solar wind interaction with Mars predicted that significant electromagnetic wave activity would be present at the interface, and within, the Martian ionosphere, as a direct result of the relatively small scale size of the magnetospheric system (Ergun et al., 2006; Kallio et al., 2011). Subsequent studies have confirmed this and hint that a plethora of electromagnetic wave modes exist and interact with the ionospheric plasma to drive energization and dynamics (e.g., Fowler et al., 2018a, 2021; Collinson et al., 2018). Several of these studies have identified the presence of whistler mode waves and subsequent wave-particle interactions in this Mars-solar wind interaction region. However, Alfvén waves have not been conclusively detected in the ionosphere or along remanent crustal magnetic fields yet. This could be due to the instrumental cadence or orbital geometry associated with previous missions to Mars as well as the lack of consistent conditions leading to their excitation.

Despite this progress, there is still much to be done to definitively identify wave modes and the processes giving rise to them at Mars. The lack of sufficient studies is partly due to the relatively small amount of simultaneous ion plasma and magnetic field data before the current MAVEN mission and the dynamics behavior of the Martian environment, among other factors. Mars possesses a hybrid magnetosphere with elements of induced and intrinsic magnetospheres (Mazelle et al., 2004; Brain et al., 2003; DiBraccio et al., 2022; Dubinin et al., 2023). The extended hydrogen corona is also responsible for additional processes and their variability over long (seasonal) timescales (Halekas, 2017; Romanelli et al., 2016; Romeo et al., 2021). Also, the use of single spacecraft observations does not allow computing the Doppler shift for low-frequency waves, due to the relative motion between the plasma rest frame and the spacecraft reference frame. Given that the solar wind velocity is close to or larger than the phase speed of many waves inside and upstream of the Martian magnetosphere, the waves are observed at different speeds and, in some cases, with different polarization than that seen in the plasma reference frame (Brinca, 1991). As a result, so far many studies on waves have investigated the conditions that favor their excitation and basic properties, such as the observed frequency and polarization, as opposed to looking at the intrinsic wave frequency and wavelength and determining the corresponding wave mode.

Future studies could be focused on the determination of the direction of the energy cascade rate upstream of Mars and the effects that PCW and foreshock waves have on the MHD and kinetic

regimes. Comparison between studies at different planetary foreshocks is also an interesting venue for future work. Moreover, an analysis of the processes occurring in the Martian bow shock and magnetic pile-up boundary would be beneficial to better understand the nature of the wave activity present inside the Martian magnetosphere, in particular the magnetosheath. Additional unknowns remain including wave mode identification downstream of the MPB and Alfvén wave detection near the ionosphere or along the crustal magnetic fields. If the latter are present, additional analyses should be focused on determining their occurrence rates (in time and space), their production mechanisms, their impacts on the local plasma, and their impact on more global parameters.

A combination of current in-situ measurements and global simulations can address some of these unknowns. Hybrid numerical simulations are particularly useful to improve data analysis and point out physical processes potentially taking place in the Martian magnetosphere (Jarvinen et al., 2022; Modolo et al., 2016; Romanelli et al., 2018c). They are also important as wave amplitudes are often large, suggesting linear wave theory is limited (if not invalid) in interpreting spacecraft observations. However, answers to some of the previous questions will likely remain elusive until measurements equivalent in capability to those made by terrestrial space physics missions can be made at Mars. In particular, simultaneous multi-spacecraft and multi-probe electric and magnetic field measurements with high-time resolution particle instruments are needed to determine the exact wave modes, polarization, and Poynting flux. These observations would allow, in turn, the determination of the growth and dissipation of waves in various regions in the Martian magnetosphere. In this regard, multi-spacecraft missions such as the planned Escape and Plasma Acceleration and Dynamics Explorers (ESCAPADE) will certainly contribute to improving our current understanding of waves in this magnetosphere (Lillis et al., 2022).

Acknowledgements

The MAVEN project is supported by NASA through the Mars Exploration Program. The material is based upon work supported by NASA under award number 80GSFC21M0002. Support for this research was also provided by GSFC/EIMM within NASA's Planetary Science Division Research Program.

References

Acuña, M. H., Connerney, J. E. P., Ness, N. F., Lin, R. P., Mitchell, D., Carlson, C. W., McFadden, J., Anderson, K. A., Reme, H., Mazelle, C., Vignes, D., Wasilewski, P., and Cloutier, P. (1999). Global Distribution of Crustal Magnetization Discovered by the Mars Global Surveyor MAG/ER Experiment. *Science*, 284:790.

Acuña, M. H., Connerney, J. E. P., Wasilewski, P., Lin, R. P., Anderson, K. A., Carlson, C. W., McFadden, J., Curtis, D. W., Mitchell, D., Reme, H., Mazelle, C., Sauvaud, J. A., d'Uston, C., Cros, A., Medale, J. L., Bauer, S. J., Cloutier, P., Mayhew, M., Winterhalter, D., and Ness, N. F. (1998). Magnetic Field and Plasma Observations at Mars: Initial Results of the Mars Global Surveyor Mission. *Science*, 279(5357):1676–1680.

Alexandrova, O. (2008). Solar wind vs magnetosheath turbulence and alfvén vortices. *Nonlinear Processes in Geophysics*, 15(1):95–108.

Alfvén, H. (1942). Existence of electromagnetic-hydrodynamic waves. *Nature*, 150(3805):405–406.

Andersson, L., Ergun, R. E., Delory, G. T., Eriksson, A., Westfall, J., Reed, H., McCauly, J., Summers, D., and Meyers, D. (2015). The Langmuir Probe and Waves (LPW) Instrument for MAVEN. *Space Science Reviews*, 195(1-4):173–198.

Andre, M. and Yau, A. (1997). Theories and Observations of Ion Energization and Outflow in the High Latitude Magnetosphere. *Space Science Reviews*, 80:27–48.

Andrés, N., Galtier, S., and Sahraoui, F. (2018). Exact law for homogeneous compressible hall magnetohydrodynamics turbulence. *Physical Review E*, 97(1):013204.

Andrés, N., Meziane, K., Mazelle, C., Bertucci, C., and Gómez, D. (2015). The ulf wave foreshock boundary: Cluster observations. *Journal of Geophysical Research: Space Physics*, 120(6):4181–4193.

Andrés, N., Mininni, P. D., Dmitruk, P., and Gomez, D. O. (2016). von kármán–howarth equation for three-dimensional two-fluid plasmas. *Physical Review E*, 93(6):063202.

Andrés, N., Romanelli, N., Hadid, L. Z., Sahraoui, F., DiBraccio, G., and Halekas, J. (2020). Solar Wind Turbulence Around Mars: Relation between the Energy Cascade Rate and the Proton Cyclotron Waves Activity. *The Astrophysical Journal*, 902(2):134.

Andrés, N., Sahraoui, F., Hadid, L. Z., Huang, S. Y., Romanelli, N., Galtier, S., DiBraccio, G., and Halekas, J. (2021). The evolution of compressible solar wind turbulence in the inner heliosphere: PSP, THEMIS, and MAVEN observations. *The Astrophysical Journal*, 919(1):19.

Auer, P. L., Kilb, R. W., and Crevier, W. F. (1971). Thermalization in the Earth's bow shock. *Journal of Geophysical Research*, 76(13):2927.

Bale, S. D., Balikhin, M. A., Horbury, T. S., Krasnoselskikh, V. V., Kucharek, H., Möbius, E., Walker, S. N., Balogh, A., Burgess, D., Lembège, B., Lucek, E. A., Scholer, M., Schwartz7 10, S. J., and Thomsen, M. F. (2005). Quasi-perpendicular Shock Structure and Processes. *Space Science Reviews*, 118(1-4):161–203.

Bandyopadhyay, R., Goldstein, M., Maruca, B., Matthaeus, W., Parashar, T., Ruffolo, D., Chhiber, R., Usmanov, A., Chasapis, A., Qudsi, R., et al. (2020). Enhanced energy transfer rate in solar wind turbulence observed near the sun from parker solar probe. *The Astrophysical Journal Supplement Series*, 246(2):48.

Barabash, S., Dubinin, E., Pissarenko, N., Lundin, R., and Russell, C. T. (1991). Picked-up protons near Mars: Phobos observations. *Geophysical Research Letters*, 18(10):1805–1808.

Bavassano, B., Pietropaolo, E., and Bruno, R. (1998). Cross-helicity and residual energy in solar wind turbulence: Radial evolution and latitudinal dependence in the region from 1 to 5 AU. *Journal of Geophysical Research*, 103(A4):6521–6530.

Belcher, J. W. and Davis, Leverett, J. (1971). Large-amplitude Alfvén waves in the interplanetary medium, 2. *Journal of Geophysical Research*, 76(16):3534.

Bertucci, C., Duru, F., Edberg, N., Fraenz, M., Martinecz, C., Szego, K., and Vaisberg, O. (2011). The Induced Magnetospheres of Mars, Venus, and Titan. *Space Science Reviews*, 162(1-4):113–171.

Bertucci, C., Romanelli, N., Chaufray, J.-Y., Gomez, D., Mazelle, C., Delva, M., Modolo, R., González-Galindo, F., and Brain, D. A. (2013). Temporal variability of waves at the proton cyclotron frequency upstream from Mars: Implications for Mars distant hydrogen exosphere. *Geophysical Research Letters*, 40(15):3809–3813.

Bhattacharyya, D., Clarke, J. T., Bertaux, J.-L., Chaufray, J.-Y., and Mayyasi, M. (2015). A strong seasonal dependence in the martian hydrogen exosphere. *Geophysical Research Letters*, 42(20):8678–8685.

Biskamp, D. (1973). Collisionless shock waves in plasmas. *Nuclear Fusion*, 13(5):719.

Bowers, C. F., DiBraccio, G. A., Slavin, J. A., Gruesbeck, J. R., Weber, T., Xu, S., Romanelli, N., and Harada, Y. (2023). Exploring the solar wind-planetary interaction at mars: Implication for magnetic reconnection. *Journal of Geophysical Research: Space Physics*, 128(2):e2022JA030989. e2022JA030989 2022JA030989.

Brain, D. A., Bagenal, F., Acuña, M. H., and Connerney, J. E. P. (2003). Martian magnetic morphology: Contributions from the solar wind and crust. *Journal of Geophysical Research: Space Physics*, 108(A12).

Brain, D. A., Bagenal, F., Acuña, M. H., Connerney, J. E. P., Crider, D. H., Mazelle, C., Mitchell, D. L., and Ness, N. F. (2002). Observations of low-frequency electromagnetic plasma waves upstream from the Martian shock. *Journal of Geophysical Research: Space Physics*, 107(A6).

Brain, D. A., Lillis, R. J., Mitchell, D. L., Halekas, J. S., and Lin, R. P. (2007). Electron pitch angle distributions as indicators of magnetic field topology near mars. *Journal of Geophysical Research: Space Physics*, 112(A9).

Brain, D. A., McFadden, J. P., Halekas, J. S., Connerney, J. E. P., Bougher, S. W., Curry, S., Dong, C. F., Dong, Y., Eparvier, F., Fang, X., Fortier, K., Hara, T., Harada, Y., Jakosky, B. M., Lillis, R. J., Livi, R., Luhmann, J. G., Ma, Y., Modolo, R., and Seki, K. (2015). The spatial distribution of planetary ion fluxes near mars observed by maven. *Geophysical Research Letters*, 42(21):9142–9148.

Breech, B., Matthaeus, W. H., Minnie, J., Oughton, S., Parhi, S., Bieber, J. W., and Bavassano, B. (2005). Radial evolution of cross helicity in high-latitude solar wind. *Geophysical Research Letters*, 32(6):L06103.

Brinca, A. (1991). Cometary linear instabilities: from profusion to perspective. *Geophysical Monograph Series*, 61:211–221.

Brinca, A. and Tsurutani, B. T. (1989). Influence of multiple ion species on low-frequency electromagnetic wave instabilities. *Journal of Geophysical Research: Space Physics*, 94(A10):13565–13569.

Bruno, R. and Carbone, V. (2013). The Solar Wind as a Turbulence Laboratory. *Living Reviews in Solar Physics*, 10(1):2.

Burch, J. L., Moore, T. E., Torbert, R. B., and Giles, B. L. (2016). Magnetospheric Multiscale Overview and Science Objectives. *Space Science Reviews*, 199(1-4):5–21.

Burgess, D., Lucek, E. A., Scholer, M., Bale, S. D., Balikhin, M. A., Balogh, A., Horbury, T. S., Krasnoselskikh, V. V., Kucharek, H., Lembège, B., Möbius, E., Schwartz, S. J., Thomsen, M. F., and Walker, S. N. (2005). Quasi-parallel Shock Structure and Processes. *Space Science Reviews*, 118(1-4):205–222.

Burgess, D., Möbius, E., and Scholer, M. (2012). Ion Acceleration at the Earth's Bow Shock. *Space Science Reviews*, 173(1-4):5–47.

Burgess, D., Wilkinson, W. P., and Schwartz, S. J. (1989). Ion distributions and thermalization at perpendicular and quasi-perpendicular supercritical collisionless shocks. *Journal of Geophysical Research*, 94(A7):8783–8792.

Carlson, C. W., Pfaff, R. F., and Watzin, J. G. (1998). The Fast Auroral SnapshoT (FAST) Mission. *Geophysical Research Letters*, 25(12):2013–2016.

Chaffin, M. S., Chaufray, J. Y., Deighan, J., Schneider, N. M., McClintock, W. E., Stewart, A. I. F., Thiemann, E., Clarke, J. T., Holsclaw, G. M., Jain, S. K., Crismani, M. M. J., Stiepen, A., Montmessin, F., Eparvier, F. G., Chamberlain, P. C., and Jakosky, B. M. (2015). Three-dimensional structure in the mars h corona revealed by iuvs on maven. *Geophysical Research Letters*, 42(21):9001–9008.

Chaffin, M. S., Kass, D. M., Aoki, S., Fedorova, A. A., Deighan, J., Connour, K., Heavens, N. G., Kleinböhl, A., Jain, S. K., Chaufray, J. Y., Mayyasi, M., Clarke, J. T., Stewart, A. I. F., Evans, J. S., Stevens, M. H., McClintock, W. E., Crismani, M. M. J., Holsclaw, G. M., Lefevre, F., Lo, D. Y., Montmessin, F., Schneider, N. M., Jakosky, B., Villanueva, G., Liuzzi, G., Daerden, F., Thomas, I. R., Lopez-Moreno, J. J., Patel, M. R., Bellucci, G., Ristic, B., Erwin, J. T., Vandaele, A. C., Trokhimovskiy, A., and Korablev, O. I. (2021). Martian water loss to space enhanced by regional dust storms. *Nature Astronomy*, 5:1036–1042.

Chen, L.-J., Halekas, J., Wang, S., DiBraccio, G. A., Romanelli, N., Ng, J., Russell, C. T., Schwartz, S. J., Sibeck, D. G., Farrell, W., Pollock, C., Gershman, D., Giles, B., and Collado-Vega, Y. M. (2022). Solitary magnetic structures developed from gyro-resonance with solar wind ions at mars and earth. *Geophysical Research Letters*, 49(3):e2021GL097600. e2021GL097600 2021GL097600.

Clarke, J. T., Mayyasi, M., Bhattacharyya, D., Schneider, N. M., Mcclintock, W. E., Deighan, J. I., Stewart, A. I. F., Chaufray, J.-Y., Chaffin, M. S., Jain, S. K., Stiepen, A., Crismani, M., Holsclaw, G. M., Montmessin, F., and Jakosky, B. M. (2017). Variability of D and H in the Martian upper atmosphere observed with the MAVEN IUVS echelle channel. *Journal of Geophysical Research: Space Physics*, 122(2):2336–2344.

Collinson, G., Wilson III, L. B., Omidi, N., Sibeck, D., Espley, J., Fowler, C. M., Mitchell, D., Grebowsky, J., Mazelle, C., Ruhunusiri, S., Halekas, J., Frahm, R., Zhang, T., Futaana, Y., and Jakosky, B. (2018). Solar wind induced waves in the skies of mars: Ionospheric compression, energization, and escape resulting from the impact of ultralow frequency magnetosonic waves generated upstream of the martian bow shock. *Journal of Geophysical Research: Space Physics*, 123(9):7241–7256.

Connerney, J. E. P., Espley, J., Lawton, P., Murphy, S., Odom, J., Oliversen, R., and Sheppard, D. (2015). The MAVEN magnetic field investigation. *Space Science Reviews*, 195(1-4):257–291.

Cramer, N. (2001). *The Physics of Alfvén Waves*. John Wiley & Sons, Ltd.

Cravens, T. and Gombosi, T. (2004). Cometary magnetospheres: a tutorial. *Advances in Space Research*, 33(11):1968–1976. Comparative Magnetospheres.

Crider, D. H., Brain, D. A., Acuña, M. H., Vignes, D., Mazelle, C., and Bertucci, C. (2004). Mars Global Surveyor Observations of Solar Wind Magnetic Field Draping Around Mars. *Space Science Reviews*, 111(1):203–221.

Curry, S. M., Luhmann, J. G., Ma, Y. J., Dong, C. F., Brain, D., Leblanc, F., Modolo, R., Dong, Y., McFadden, J., Halekas, J., Connerney, J., Espley, J., Hara, T., Harada, Y., Lee, C., Fang, X., and Jakosky, B. (2015). Response of Mars O+ pickup ions to the 8 March 2015 ICME: Inferences from MAVEN data-based models. *Geophysical Research Letters*, 42(21):9095–9102.

Curry, S. M., Tatum, P., Mitchell, D., Luhmann, J. G., McFadden, J., Ruhunusiri, S., DiBraccio, G., Ramstad, R., and Xu, S. (2022). Ion acceleration in Mars' twisted magnetotail. *Monthly Notices of the Royal Astronomical Society: Letters*, 517(1):L121–L125.

Deighan, J., Chaffin, M. S., Chaufray, J.-Y., Stewart, A. I. F., Schneider, N. M., Jain, S. K., Stiepen, A., Crismani, M., McClintock, W. E., Clarke, J. T., Holsclaw, G. M., Montmessin, F., Eparvier, F. G., Thiemann, E. M. B., Chamberlin, P. C., and Jakosky, B. M. (2015).

MAVEN IUVS observation of the hot oxygen corona at Mars. *Geophysical Research Letters*, 42(21):9009–9014.

Delva, M., Bertucci, C., Volwerk, M., Lundin, R., Mazelle, C., and Romanelli, N. (2015). Upstream proton cyclotron waves at venus near solar maximum. *Journal of Geophysical Research: Space Physics*, 120(1):344–354.

Delva, M. and Dubinin, E. (1998). Upstream ulf fluctuations near mars. *Journal of Geophysical Research: Space Physics*, 103(A1):317–326.

Delva, M., Mazelle, C., and Bertucci, C. (2011). Upstream Ion Cyclotron Waves at Venus and Mars. *Space Science Reviews*, 162(1-4):5–24.

DiBraccio, G. A., Dann, J., Espley, J. R., Gruesbeck, J. R., Soobiah, Y., Connerney, J. E. P., Halekas, J. S., Harada, Y., Bowers, C. F., Brain, D. A., Ruhunusiri, S., Hara, T., and Jakosky, B. M. (2017). Maven observations of tail current sheet flapping at mars. *Journal of Geophysical Research: Space Physics*, 122(4):4308–4324.

DiBraccio, G. A., Luhmann, J. G., Curry, S. M., Espley, J. R., Xu, S., Mitchell, D. L., Ma, Y., Dong, C., Gruesbeck, J. R., Connerney, J. E. P., Harada, Y., Ruhunusiri, S., Halekas, J. S., Soobiah, Y., Hara, T., Brain, D. A., and Jakosky, B. M. (2018). The twisted configuration of the martian magnetotail: Maven observations. *Geophysical Research Letters*, 45(10):4559–4568.

DiBraccio, G. A., Romanelli, N., Bowers, C. F., Gruesbeck, J. R., Halekas, J. S., Ruhunusiri, S., Weber, T., Espley, J. R., Xu, S., Luhmann, J. G., Harada, Y., Dubinin, E., Poh, G. K., Brain, D. A., and Curry, S. M. (2022). A statistical investigation of factors influencing the magnetotail twist at mars. *Geophysical Research Letters*, 49(12):e2022GL098007. e2022GL098007 2022GL098007.

Dong, Y., Fang, X., Brain, D. A., McFadden, J. P., Halekas, J. S., Connerney, J. E., Curry, S. M., Harada, Y., Luhmann, J. G., and Jakosky, B. M. (2015). Strong plume fluxes at Mars observed by MAVEN: An important planetary ion escape channel. *Geophysical Research Letters*, 42(21):8942–8950.

Dubinin, E. and Fraenz, M. (2016). *Ultra-Low-Frequency Waves at Venus and Mars*, chapter 20, pages 343–364. American Geophysical Union (AGU).

Dubinin, E., Fraenz, M., Fedorov, A., Lundin, R., Edberg, N., Duru, F., and Vaisberg, O. (2011). Ion Energization and Escape on Mars and Venus. *Space Science Reviews*, 162(1-4):173–211.

Dubinin, E., Fraenz, M., Pätzold, M., Halekas, J. S., Mcfadden, J., Connerney, J. E. P., Jakosky, B. M., Vaisberg, O., and Zelenyi, L. (2018). Solar wind deflection by mass loading in the martian magnetosheath based on maven observations. *Geophysical Research Letters*, 45(6):2574–2579.

Dubinin, E., Fraenz, M., Pätzold, M., Tellmann, S., Modolo, R., DiBraccio, G., McFadden, J., and Espley, J. (2023). Magnetic fields and plasma motions in a hybrid martian magnetosphere. *Journal of Geophysical Research: Space Physics*, 128(1):e2022JA030575. e2022JA030575 2022JA030575.

Dubinin, E., Fränz, M., Woch, J., Roussos, E., Barabash, S., Lundin, R., Winningham, J. D., Frahm, R. A., and Acuña, M. (2006). Plasma Morphology at Mars. Aspera-3 Observations. *Space Science Reviews*, 126(1-4):209–238.

Eastwood, J. P., Lucek, E. A., Mazelle, C., Meziane, K., Narita, Y., Pickett, J., and Treumann, R. A. (2005). The Foreshock. *Space Science Reviews*, 118(1-4):41–94.

Edberg, N. J. T., Auster, U., Barabash, S., Bößwetter, A., Brain, D. A., Burch, J. L., Carr, C. M., Cowley, S. W. H., Cupido, E., Duru, F., Eriksson, A. I., Fränz, M., Glassmeier, K. H., Goldstein, R., Lester, M., Lundin, R., Modolo, R., Nilsson, H., Richter, I., Samara, M., and Trotignon, J. G. (2009a). Rosetta and Mars Express observations of the influence of high solar wind pressure on the Martian plasma environment. *Annales Geophysicae*, 27(12):4533–4545.

Edberg, N. J. T., Brain, D. A., Lester, M., Cowley, S. W. H., Modolo, R., Fränz, M., and Barabash, S. (2009b). Plasma boundary variability at Mars as observed by Mars Global Surveyor and Mars Express. *Annales Geophysicae*, 27(9):3537–3550.

Edmiston, J. P. and Kennel, C. F. (1984). A parametric survey of the first critical mach number for a fast mhd shock. *Journal of Plasma Physics*, 32(3):429–441.

Ergun, R. E., Andersson, L., Peterson, W. K., Brain, D., Delory, G. T., Mitchell, D. L., Lin, R. P., and Yau, A. W. (2006). Role of plasma waves in mars' atmospheric loss. *Geophysical Research Letters*, 33(14).

Ergun, R. E., Andersson, L. A., Fowler, C. M., Woodson, A. K., Weber, T. D., Delory, G. T., Andrews, D. J., Eriksson, A. I., McEnulty, T., Morooka, M. W., Stewart, A. I. F., Mahaffy,

P., and Jakosky, B. M. (2016). Enhanced o2+ loss at mars due to an ambipolar electric field from electron heating. *Journal of Geophysical Research: Space Physics*, 121(5):4668–4678.

Escoubet, C. P., Schmidt, R., and Goldstein, M. L. (1997). Cluster - Science and Mission Overview. *Space Science Reviews*, 79:11–32.

Esman, T. M., Espley, J., Gruesbeck, J., Fowler, C. M., Xu, S., Elrod, M., Harada, Y., and Giacalone, J. (2022). Martian ionospheric magnetic fluctuations below 200 km. *Journal of Geophysical Research: Space Physics*, 127(9):e2022JA030470. e2022JA030470 2022JA030470.

Espley, J. R. (2018). The martian magnetosphere: Areas of unsettled terminology. *Journal of Geophysical Research: Space Physics*, 123(6):4521–4525.

Espley, J. R., Cloutier, P. A., Brain, D. A., Crider, D. H., and Acuña, M. H. (2004). Observations of low-frequency magnetic oscillations in the martian magnetosheath, magnetic pileup region, and tail. *Journal of Geophysical Research: Space Physics*, 109(A7).

Fairfield, D. H. (1971). Average and unusual locations of the earth's magnetopause and bow shock. *Journal of Geophysical Research (1896-1977)*, 76(28):6700–6716.

Feldman, P. D., Steffl, A. J., Parker, J. W., A'Hearn, M. F., Bertaux, J.-L., Alan Stern, S., Weaver, H. A., Slater, D. C., Versteeg, M., Throop, H. B., Cunningham, N. J., and Feaga, L. M. (2011). Rosetta-Alice observations of exospheric hydrogen and oxygen on Mars. *Icarus*, 214(2):394 – 399.

Ferrand, R., Galtier, S., and Sahraoui, F. (2021). A compact exact law for compressible isothermal hall magnetohydrodynamic turbulence. *Journal of Plasma Physics*, 87(2).

Formisano, V. (1979). Orientation and shape of the earth's bow shock in three dimensions. *Planetary and Space Science*, 27(9):1151–1161.

Fowler, C. M., Agapitov, O. V., Xu, S., Mitchell, D. L., Andersson, L., Artemyev, A., Espley, J., Ergun, R. E., and Mazelle, C. (2020). Localized heating of the martian topside ionosphere through the combined effects of magnetic pumping by large-scale magnetosonic waves and pitch angle diffusion by whistler waves. *Geophysical Research Letters*, 47(5):e2019GL086408. e2019GL086408 10.1029/2019GL086408.

Fowler, C. M., Andersson, L., Ergun, R. E., Harada, Y., Hara, T., Collinson, G., Peterson, W. K., Espley, J., Halekas, J., Mcfadden, J., Mitchell, D. L., Mazelle, C., Benna, M., and

Jakosky, B. M. (2018a). Maven observations of solar wind-driven magnetosonic waves heating the martian dayside ionosphere. *Journal of Geophysical Research: Space Physics*, 123(5):4129–4149.

Fowler, C. M., Andersson, L., Halekas, J., Espley, J. R., Mazelle, C., Coughlin, E. R., Ergun, R. E., Andrews, D. J., Connerney, J. E. P., and Jakosky, B. (2017). Electric and magnetic variations in the near-mars environment. *Journal of Geophysical Research: Space Physics*, 122(8):8536–8559.

Fowler, C. M., Andersson, L., Peterson, W. K., Halekas, J., Nagy, A. F., Ergun, R. E., Espley, J., Mitchell, D. L., Connerney, J. E. P., Mazelle, C., Mahaffy, P. R., and Jakosky, B. M. (2018b). Correlations between enhanced electron temperatures and electric field wave power in the martian ionosphere. *Geophysical Research Letters*, 45(2):493–501.

Fowler, C. M., Hanley, K. G., McFadden, J. P., Chaston, C. C., Bonnell, J. W., Halekas, J. S., Espley, J. R., DiBraccio, G. A., Schwartz, S. J., Mazelle, C., Mitchell, D. L., Xu, S., and Lillis, R. J. (2021). Maven observations of low frequency steepened magnetosonic waves and associated heating of the martian nightside ionosphere. *Journal of Geophysical Research: Space Physics*, 126(10):e2021JA029615. e2021JA029615 2021JA029615.

Fox, J. L. and Bakalian, F. M. (2001). Photochemical escape of atomic carbon from mars. *Journal of Geophysical Research: Space Physics*, 106(A12):28785–28795.

Frisch, U. (1995). *Turbulence. The legacy of A.N. Kolmogorov.*

Galtier, S. (2008). von kármán–howarth equations for hall magnetohydrodynamic flows. *Physical Reviw E*, 77(1):015302.

Gary, S. P. (1993). *Theory of space plasma microinstabilities.* Cambridge Atmospheric and Space Science Series. Cambridge Univ. Press.

Gary, S. P., Akimoto, K., and Winske, D. (1989). Computer simulations of cometary-ion/ion instabilities and wave growth. *Journal of Geophysical Research: Space Physics*, 94(A4):3513–3525.

Glass, A. N., Tracy, P. J., Raines, J. M., Jia, X., Romanelli, N., and DiBraccio, G. A. (2023). Characterization of foreshock plasma populations at mercury. *Journal of Geophysical Research: Space Physics*, 128(2):e2022JA031111. e2022JA031111 2022JA031111.

Glassmeier, K.-H. and Espley, J. (2006). *ULF Waves in Planetary Magnetospheres*, pages 341–359. American Geophysical Union (AGU).

Gosling, J. T. and Robson, A. E. (1985). *Ion Reflection, Gyration, and Dissipation at Supercritical Shocks*, pages 141–152. American Geophysical Union (AGU).

Gosling, J. T., Thomsen, M. F., Bame, S. J., Feldman, W. C., Paschmann, G., and Sckopke, N. (1982). Evidence for specularly reflected ions upstream from the quasi-parallel bow shock. *Geophysical Research Letters*, 9(12):1333–1336.

Grard, R., Pedersen, A., Klimov, S., Savin, S., Skalsky, A., Trotignon, J. G., and Kennel, C. (1989). First measurements of plasma waves near Mars. *Nature*, 341(6243):607–609.

Gruesbeck, J. R., Espley, J. R., Connerney, J. E. P., DiBraccio, G. A., Soobiah, Y. I., Brain, D., Mazelle, C., Dann, J., Halekas, J., and Mitchell, D. L. (2018). The three-dimensional bow shock of mars as observed by maven. *Journal of Geophysical Research: Space Physics*, 123(6):4542–4555.

Gurnett, D. A., Kirchner, D. L., Huff, R. L., Morgan, D. D., Persoon, A. M., Averkamp, T. F., Duru, F., Nielsen, E., Safaeinili, A., Plaut, J. J., and Picardi, G. (2005). Radar soundings of the ionosphere of mars. *Science*, 310(5756):1929–1933.

Gurnett, D. A., Morgan, D. D., Duru, F., Akalin, F., Winningham, J. D., Frahm, R. A., Dubinin, E., and Barabash, S. (2010). Large density fluctuations in the martian ionosphere as observed by the Mars Express radar sounder. *Icarus*, 206(1):83–94.

Hadid, L., Sahraoui, F., and Galtier, S. (2017). Energy cascade rate in compressible fast and slow solar wind turbulence. *The Astrophysical Journal*, 838(1):9.

Hadid, L. Z., Sahraoui, F., Kiyani, K. H., Retinò, A., Modolo, R., Canu, P., Masters, A., and Dougherty, M. K. (2015). Nature of the MHD and Kinetic Scale Turbulence in the Magnetosheath of Saturn: Cassini Observations. *Astrophysical Journal Letters*, 813(2):L29.

Halekas, J. S. (2017). Seasonal variability of the hydrogen exosphere of mars. *Journal of Geophysical Research: Planets*, 122(5):901–911.

Halekas, J. S., Luhmann, J. G., Dubinin, E., and Ma, Y. (2021). *Induced Magnetospheres*, chapter 25, pages 391–406. American Geophysical Union (AGU).

Halekas, J. S., Ruhunusiri, S., Harada, Y., Collinson, G., Mitchell, D. L., Mazelle, C., McFadden, J. P., Connerney, J. E. P., Espley, J. R., Eparvier, F., Luhmann, J. G., and Jakosky, B. M. (2017). Structure, dynamics, and seasonal variability of the mars-solar wind interaction: Maven solar wind ion analyzer in-flight performance and science results. *Journal of Geophysical Research: Space Physics*, 122(1):547–578.

Halekas, J. S., Ruhunusiri, S., Vaisberg, O. L., Harada, Y., Espley, J. R., Mitchell, D. L., Mazelle, C., Romanelli, N., DiBraccio, G. A., and Brain, D. A. (2020). Properties of plasma waves observed upstream from mars. *Journal of Geophysical Research: Space Physics*, 125(9):e2020JA028221. e2020JA028221 2020JA028221.

Halekas, J. S., Taylor, E. R., Dalton, G., Johnson, G., Curtis, D. W., McFadden, J. P., Mitchell, D. L., Lin, R. P., and Jakosky, B. M. (2015). The solar wind ion analyzer for MAVEN. *Space Science Reviews*, 195(1-4):125–151.

Hanley, K. G., Fowler, C. M., McFadden, J. P., Mitchell, D. L., and Curry, S. (2022). Maven-static observations of ion temperature and initial ion acceleration in the martian ionosphere. *Geophysical Research Letters*, 49(18):e2022GL100182. e2022GL100182 2022GL100182.

Harada, Y., Andersson, L., Fowler, C. M., Mitchell, D. L., Halekas, J. S., Mazelle, C., Espley, J., DiBraccio, G. A., McFadden, J. P., Brain, D. A., Xu, S., Ruhunusiri, S., Larson, D. E., Lillis, R. J., Hara, T., Livi, R., and Jakosky, B. M. (2016). Maven observations of electron-induced whistler mode waves in the martian magnetosphere. *Journal of Geophysical Research: Space Physics*, 121(10):9717–9731.

Harada, Y., Halekas, J. S., DiBraccio, G. A., Xu, S., Espley, J., Mcfadden, J. P., Mitchell, D. L., Mazelle, C., Brain, D. A., Hara, T., Ma, Y. J., Ruhunusiri, S., and Jakosky, B. M. (2018). Magnetic reconnection on dayside crustal magnetic fields at mars: Maven observations. *Geophysical Research Letters*, 45(10):4550–4558.

Harada, Y., Halekas, J. S., McFadden, J. P., Mitchell, D. L., Mazelle, C., Connerney, J. E. P., Espley, J., Larson, D. E., Brain, D. A., Andersson, L., DiBraccio, G. A., Collinson, G. A., Livi, R., Hara, T., Ruhunusiri, S., and Jakosky, B. M. (2015). Magnetic reconnection in the near-mars magnetotail: Maven observations. *Geophysical Research Letters*, 42(21):8838–8845.

Harada, Y., Ruhunusiri, S., Halekas, J. S., Espley, J., DiBraccio, G. A., Mcfadden, J. P., Mitchell, D. L., Mazelle, C., Collinson, G., Brain, D. A., Hara, T., Nosé, M., Oimatsu, S., Yamamoto,

K., and Jakosky, B. M. (2019). Locally generated ulf waves in the martian magnetosphere: Maven observations. *Journal of Geophysical Research: Space Physics*, 124(11):8707–8726.

Hughes, A., Chaffin, M., Mierkiewicz, E., Deighan, J., Jain, S., Schneider, N., Mayyasi, M., and Jakosky, B. (2019). Proton aurora on mars: A dayside phenomenon pervasive in southern summer. *Journal of Geophysical Research: Space Physics*, 124(12):10533–10548.

Jakosky, B. M., Lin, R., Grebowsky, J., Luhmann, J., Mitchell, D., Beutelschies, G., Priser, T., Acuña, M., Andersson, L., Baird, D., et al. (2015). The mars atmosphere and volatile evolution (maven) mission. *Space Science Reviews*, 195(1-4):3–48.

Jarvinen, R., Kallio, E., and Pulkkinen, T. I. (2022). Ultra-low frequency foreshock waves and ion dynamics at mars. *Journal of Geophysical Research: Space Physics*, 127(5):e2021JA030078. e2021JA030078 2021JA030078.

Jiang, W., Li, H., Liu, X., Verscharen, D., and Wang, C. (2023). Statistical properties of plateau-like turbulence spectra in the martian magnetosheath: Maven observations. *Journal of Geophysical Research: Space Physics*, 128(1):e2022JA030874. e2022JA030874 2022JA030874.

Jin, T., Lei, L., Yiteng, Z., Lianghai, X., and Fuhao, Q. (2022). Statistical analysis of the distribution and evolution of mirror structures in the martian magnetosheath. *The Astrophysical Journal*, 929(2):165.

Johnson, C. L., Mittelholz, A., Langlais, B., Russell, C. T., Ansan, V., Banfield, D., Chi, P. J., Fillingim, M. O., Forget, F., Haviland, H. F., Golombek, M., Joy, S., Lognonné, P., Liu, X., Michaut, C., Pan, L., Quantin-Nataf, C., Spiga, A., Stanley, S., Thorne, S. N., Wieczorek, M. A., Yu, Y., Smrekar, S. E., and Banerdt, W. B. (2020). Crustal and time-varying magnetic fields at the InSight landing site on Mars. *Nature Geoscience*, 13(3):199–204.

Kallio, E., Chaufray, J.-Y., Modolo, R., Snowden, D., and Winglee, R. (2011). Modeling of Venus, Mars, and Titan. *Space Science Reviews*, 162(1-4):267–307.

Kennel, C. F. and Petschek, H. E. (1966). Limit on stably trapped particle fluxes. *Journal of Geophysical Research (1896-1977)*, 71(1):1–28.

Kivelson, M. G. and Russell, C. T. (1995). *Introduction to Space Physics*.

LeDocq, M. J., Gurnett, D. A., and Hospodarsky, G. B. (1998). Chorus source locations from vlf poynting flux measurements with the polar spacecraft. *Geophysical Research Letters*, 25(21):4063–4066.

Liemohn, M. W., Mitchell, D. L., Nagy, A. F., Fox, J. L., Reimer, T. W., and Ma, Y. (2003). Comparisons of electron fluxes measured in the crustal fields at mars by the mgs magnetometer/electron reflectometer instrument with a b field–dependent transport code. *Journal of Geophysical Research: Planets*, 108(E12).

Lillis, R., Curry, S., Hara, T., Curtis, D., Taylor, E., Parker, J., Luhmann, J. G., Barjatya, A., Larson, D., Livi, R., Whittlesey, P., Ma, Y., Harada, Y., Modolo, R., Thiemann, E., and Brain, D. (2022). ESCAPADE: Mars' first smallsat science mission will unveil its unique hybrid magnetosphere. In *44th COSPAR Scientific Assembly. Held 16-24 July*, volume 44, page 420.

Lillis, R. J., Deighan, J., Fox, J. L., Bougher, S. W., Lee, Y., Combi, M. R., Cravens, T. E., Rahmati, A., Mahaffy, P. R., Benna, M., Elrod, M. K., McFadden, J. P., Ergun, R. E., Andersson, L., Fowler, C. M., Jakosky, B. M., Thiemann, E., Eparvier, F., Halekas, J. S., Leblanc, F., and Chaufray, J.-Y. (2017). Photochemical escape of oxygen from mars: First results from maven in situ data. *Journal of Geophysical Research: Space Physics*, 122(3):3815–3836.

Liu, D., Yao, Z., Wei, Y., Rong, Z., Shan, L., Arnaud, S., Espley, J., Wei, H., and Wan, W. (2020). Upstream proton cyclotron waves: occurrence and amplitude dependence on imf cone angle at mars—from maven observations. *Earth and Planetary Physics*, 4(1):51–61.

Livesey, W. A., Kennel, C. F., and Russell, C. T. (1982). ISEE-1 and -2 observations of magnetic field strength overshoots in quasi-perpendicular bow shocks. *Geophysical Research Letters*, 9(9):1037–1040.

Maron, J. and Goldreich, P. (2001). Simulations of Incompressible Magnetohydrodynamic Turbulence. *The Astrophysical Journal*, 554(2):1175–1196.

Mazelle, C., Winterhalter, D., Sauer, K., Trotignon, J. G., Acuna, M. H., Baumgärtel, K., Bertucci, C., Brain, D. A., Brecht, S. H., Delva, M., Dubinin, E., Øieroset, M., and Slavin, J. (2004). Bow shock and upstream phenomena at mars. *Space Science Reviews*, 111:115–181.

McFadden, J. P., Kortmann, O., Curtis, D., Dalton, G., Johnson, G., Abiad, R., Sterling, R., Hatch, K., Berg, P., Tiu, C., Gordon, D., Heavner, S., Robinson, M., Marckwordt, M., Lin, R., and Jakosky, B. (2015). MAVEN SupraThermal and Thermal Ion Compostion (STATIC) Instrument. *Space Science Reviews*, 195(1-4):199–256.

Meziane, K., Mazelle, C. X., Romanelli, N., Mitchell, D. L., Espley, J. R., Connerney, J. E. P., Hamza, A. M., Halekas, J., McFadden, J. P., and Jakosky, B. M. (2017). Martian electron foreshock from maven observations. *Journal of Geophysical Research: Space Physics*, 122(2):1531–1541.

Mitchell, D. L., Mazelle, C., Sauvaud, J. A., Thocaven, J. J., Rouzaud, J., Fedorov, A., Rouger, P., Toublanc, D., Taylor, E., Gordon, D., Robinson, M., Heavner, S., Turin, P., Diaz-Aguado, M., Curtis, D. W., Lin, R. P., and Jakosky, B. M. (2016). The MAVEN Solar Wind Electron Analyzer. *Space Science Reviews*, 200(1-4):495–528.

Mittelholz, A., Johnson, C. L., Fillingim, M., Grimm, R. E., Joy, S., Thorne, S. N., and Banerdt, W. B. (2023). Mars' external magnetic field as seen from the surface with insight. *Journal of Geophysical Research: Planets*, 128(1):e2022JE007616. e2022JE007616 2022JE007616.

Mittelholz, A., Johnson, C. L., Fillingim, M., Joy, S. P., Espley, J., Halekas, J., Smrekar, S., and Banerdt, W. B. (2021). Space weather observations with insight. *Geophysical Research Letters*, 48(22):e2021GL095432. e2021GL095432 2021GL095432.

Modolo, R., Hess, S., Mancini, M., Leblanc, F., Chaufray, J.-Y., Brain, D., Leclercq, L., Esteban-Hernández, R., Chanteur, G., Weill, P., González-Galindo, F., Forget, F., Yagi, M., and Mazelle, C. (2016). Mars-solar wind interaction: Lathys, an improved parallel 3-d multispecies hybrid model. *Journal of Geophysical Research: Space Physics*, 121(7):6378–6399.

Moses, S. L., Coroniti, F. V., and Scarf, F. L. (1988). Expectations for the microphysics of the Mars-solar wind interaction. *Geophysical Research Letters*, 15(5):429–432.

Nagy, A. F., Winterhalter, D., Sauer, K., Cravens, T. E., Brecht, S., Mazelle, C., Crider, D., Kallio, E., Zakharov, A., Dubinin, E., Verigin, M., Kotova, G., Axford, W. I., Bertucci, C., and Trotignon, J. G. (2004). The plasma Environment of Mars. *Space Science Reviews*, 111(1):33–114.

Orosei, R., Jordan, R. L., Morgan, D. D., Cartacci, M., Cicchetti, A., Duru, F., Gurnett, D. A., Heggy, E., Kirchner, D. L., Noschese, R., Kofman, W., Masdea, A., Plaut, J. J., Seu, R., Watters, T. R., and Picardi, G. (2015). Mars Advanced Radar for Subsurface and Ionospheric Sounding (MARSIS) after nine years of operation: A summary. *Planetary and Space Science*, 112:98–114.

Papadopoulos, K. (1971). Ion thermalization in the Earth's bow shock. *Journal of Geophysical Research*, 76(16):3806.

Parker, E. N. (1958). Dynamics of the Interplanetary Gas and Magnetic Fields. *The Astrophysical Journal*, 128:664.

Paschmann, G., Sckopke, N., Asbridge, J., Bame, S., and Gosling, J. (1980). Energization of solar wind ions by reflection from the earth's bow shock. *Journal of Geophysical Research: Space Physics*, 85(A9):4689–4693.

Paschmann, G., Sckopke, N., Papamastorakis, I., Asbridge, J. R., Bame, S. J., and Gosling, J. T. (1981). Characteristics of reflected and diffuse ions upstream from the earth's bow shock. *Journal of Geophysical Research*, 86(A6):4355–4364.

Phillips, P. E. and Robson, A. E. (1972). Influence of Reflected Ions on the Magnetic Structure of a Collisionless Shock Front. *Physical Review Letters*, 29(3):154–157.

Picardi, G., Biccari, D., Seu, R., Marinangeli, L., Johnson, W. T. K., Jordan, R. L., Plaut, J., Safaenili, A., Gurnett, D. A., Ori, G. G., Orosei, R., Calabrese, D., and Zampolini, E. (2004). Performance and surface scattering models for the Mars Advanced Radar for Subsurface and Ionosphere Sounding (MARSIS). *Planetary and Space Science*, 52:149–156.

Politano, H. and Pouquet, A. (1998a). Dynamical length scales for turbulent magnetized flows. *Geophysical Research Letters*, 25(3):273–276.

Politano, H. and Pouquet, A. (1998b). von kármán–howarth equation for magnetohydrodynamics and its consequences on third-order longitudinal structure and correlation functions. *Physical Review E*, 57(1):R21.

Pope, S. B. (2001). Turbulent flows.

Rahmati, A., Larson, D. E., Cravens, T. E., Lillis, R. J., Dunn, P. A., Halekas, J. S., Connerney, J. E., Eparvier, F. G., Thiemann, E. M. B., and Jakosky, B. M. (2015). MAVEN insights into oxygen pickup ions at Mars. *Geophysical Research Letters*, 42(21):8870–8876.

Rahmati, A., Larson, D. E., Cravens, T. E., Lillis, R. J., Halekas, J. S., McFadden, J. P., Dunn, P. A., Mitchell, D. L., Thiemann, E. M. B., Eparvier, F. G., DiBraccio, G. A., Espley, J. R., Mazelle, C., and Jakosky, B. M. (2017). Maven measured oxygen and hydrogen pickup ions: Probing the martian exosphere and neutral escape. *Journal of Geophysical Research: Space Physics*, 122(3):3689–3706.

Rahmati, A., Larson, D. E., Cravens, T. E., Lillis, R. J., Halekas, J. S., McFadden, J. P., Mitchell, D. L., Thiemann, E. M. B., Connerney, J. E. P., Dunn, P. A., Lee, C. O., Eparvier,

F. G., DiBraccio, G. A., Espley, J. R., Luhmann, J. G., Mazelle, C., and Jakosky, B. M. (2018). Seasonal variability of neutral escape from mars as derived from maven pickup ion observations. *Journal of Geophysical Research: Planets*, 123(5):1192–1202.

Ramstad, R., Barabash, S., Futaana, Y., Nilsson, H., Wang, X.-D., and Holmström, M. (2015). The martian atmospheric ion escape rate dependence on solar wind and solar euv conditions: 1. seven years of mars express observations. *Journal of Geophysical Research: Planets*, 120(7):1298–1309.

Ramstad, R., Brain, D. A., Dong, Y., Espley, J., Halekas, J., and Jakosky, B. (2020). The global current systems of the Martian induced magnetosphere. *Nature Astronomy*, 4:979–985.

Roberts, D. A., Goldstein, M. L., Klein, L. W., and Matthaeus, W. H. (1987). Origin and evolution of fluctuations in the solar wind: Helios observations and helios-voyager comparisons. *Journal of Geophysical Research: Space Physics*, 92(A11):12023–12035.

Romanelli, N., Andrés, N., and DiBraccio, G. A. (2022). Variability of the incompressible energy cascade rate in solar wind turbulence around mars. *The Astrophysical Journal*, 929(2):145.

Romanelli, N., Bertucci, C., Gomez, D., Mazelle, C., and Delva, M. (2013). Proton cyclotron waves upstream from mars: Observations from mars global surveyor. *Planetary and Space Science*, 76:1–9.

Romanelli, N., Bertucci, C., Gómez, D., and Mazelle, C. (2015). Dependence of the location of the martian magnetic lobes on the interplanetary magnetic field direction: Observations from mars global surveyor. *Journal of Geophysical Research: Space Physics*, 120(9):7737–7747.

Romanelli, N., DiBraccio, G., Gershman, D., Le, G., Mazelle, C., Meziane, K., Boardsen, S., Slavin, J., Raines, J., Glass, A., and Espley, J. (2020a). Upstream ultra-low frequency waves observed by messenger's magnetometer: Implications for particle acceleration at mercury's bow shock. *Geophysical Research Letters*, 47(9):e2020GL087350. e2020GL087350 10.1029/2020GL087350.

Romanelli, N., DiBraccio, G., Halekas, J., Dubinin, E., Gruesbeck, J., Espley, J., Poh, G., Ma, Y., and Luhmann, J. G. (2020b). Variability of the solar wind flow asymmetry in the martian magnetosheath observed by maven. *Geophysical Research Letters*, 47(22):e2020GL090793. e2020GL090793 10.1029/2020GL090793.

Romanelli, N., DiBraccio, G., Modolo, R., Leblanc, F., Espley, J., Gruesbeck, J., Halekas, J., Mcfadden, J., and Jakosky, B. (2019). Recovery timescales of the dayside martian magnetosphere to imf variability. *Geophysical Research Letters*, 46(20):10977–10986.

Romanelli, N. and DiBraccio, G. A. (2021). Occurrence rate of ultra-low frequency waves in the foreshock of Mercury increases with heliocentric distance. *Nature Communications*, 12:6748.

Romanelli, N., Gómez, D., Bertucci, C., and Delva, M. (2014). Steady-state Magnetohydrodynamic Flow around an Unmagnetized Conducting Sphere. *The Astrophysical Journal*, 789(1):43.

Romanelli, N., Mazelle, C., Chaufray, J.-Y., Meziane, K., Shan, L., Ruhunusiri, S., Connerney, J. E., Espley, J. R., Eparvier, F., Thiemann, E., et al. (2016). Proton cyclotron waves occurrence rate upstream from mars observed by maven: Associated variability of the martian upper atmosphere. *Journal of Geophysical Research: Space Physics*, 121(11):11–113.

Romanelli, N., Mazelle, C., and Meziane, K. (2018a). Nonlinear wave-particle interaction: Implications for newborn planetary and backstreaming proton velocity distribution functions. *Journal of Geophysical Research: Space Physics*, 123:1100–1117.

Romanelli, N., Modolo, R., Leblanc, F., Chaufray, J.-Y., Hess, S., Brain, D., Connerney, J., Halekas, J., Mcfadden, J., and Jakosky, B. (2018b). Effects of the crustal magnetic fields and changes in the imf orientation on the magnetosphere of mars: Maven observations and lathys results. *Journal of Geophysical Research: Space Physics*, 123(7):5315–5333.

Romanelli, N., Modolo, R., Leblanc, F., Chaufray, J.-Y., Martinez, A., Ma, Y., Lee, C. O., Luhmann, J. G., Halekas, J., Brain, D., DiBraccio, G., Espley, J., Mcfadden, J., Jakosky, B., and Holmström, M. (2018c). Responses of the Martian Magnetosphere to an Interplanetary Coronal Mass Ejection: MAVEN Observations and LatHyS Results. *Geophysical Research Letters*, 45(16):7891–7900.

Romeo, O. M., Romanelli, N., Espley, J. R., Mazelle, C., DiBraccio, G. A., Gruesbeck, J. R., and Halekas, J. S. (2021). Variability of upstream proton cyclotron wave properties and occurrence at mars observed by maven. *Journal of Geophysical Research: Space Physics*, 126(2):e2020JA028616. e2020JA028616 2020JA028616.

Ruhunusiri, S., Halekas, J., Espley, J., Mazelle, C., Brain, D., Harada, Y., DiBraccio, G., Livi, R., Larson, D., Mitchell, D., et al. (2017). Characterization of turbulence in the mars plasma

environment with maven observations. *Journal of Geophysical Research: Space Physics*, 122(1):656–674.

Ruhunusiri, S., Halekas, J. S., Connerney, J. E. P., Espley, J. R., McFadden, J. P., Larson, D. E., Mitchell, D. L., Mazelle, C., and Jakosky, B. M. (2015). Low-frequency waves in the martian magnetosphere and their response to upstream solar wind driving conditions. *Geophysical Research Letters*, 42(21):8917–8924.

Russell, C. T. (1994). *Planetary Upstream Waves*, pages 75–86. American Geophysical Union (AGU).

Russell, C. T., Luhmann, J. G., Schwingenschuh, K., Riedler, W., and Yeroshenko, Y. (1990). Upstream waves at mars: Phobos observations. *Geophysical Research Letters*, 17(6):897–900.

Shane, A. and Liemohn, M. (2021). Whistler wave interactions with superthermal electrons on martian crustal magnetic fields: Bounce-averaged diffusion coefficients and time scales. *Journal of Geophysical Research: Space Physics*, 126(6):e2021JA029118. e2021JA029118 2021JA029118.

Shane, A., Liemohn, M., Florie, C., and Xu, S. (2019). Misbehaving high-energy electrons: Evidence in support of ubiquitous wave-particle interactions on dayside martian closed crustal magnetic fields. *Geophysical Research Letters*, 46(21):11689–11697.

Shane, A. D. and Liemohn, M. W. (2022). Modeling wave-particle interactions with photoelectrons on the dayside crustal fields of mars. *Geophysical Research Letters*, 49(2):e2021GL096941. e2021GL096941 2021GL096941.

Simon-Wedlund, C., Volwerk, M., Mazelle, C., Halekas, J., Rojas-Castillo, D., Espley, J., and Möstl, C. (2022a). Making waves: Mirror mode structures around mars observed by the maven spacecraft. *Journal of Geophysical Research: Space Physics*, 127(1):e2021JA029811. e2021JA029811 2021JA029811.

Simon-Wedlund, C., Volwerk, M., Mazelle, C., Rojas Mata, S., Stenberg Wieser, G., Futaana, Y., Halekas, J., Rojas-Castillo, D., Bertucci, C., and Espley, J. (2022b). Statistical distribution of mirror mode-like structures in the magnetosheaths of unmagnetised planets: 1. mars as observed by the maven spacecraft. *EGUsphere*, 2022:1–40.

Skalsky, A., Dubinin, E., Delva, M., Grard, R., Klimov, S., Sauer, K., and Trotignon, J. G.

(1998). Wave observations at the foreshock boundary in the near-Mars space. *Earth, Planets and Space*, 50:439–444.

Slavin, J. A. and Holzer, R. E. (1981). Solar wind flow about the terrestrial planets 1. Modeling bow shock position and shape. *Journal of Geophysical Research*, 86(A13):11401.

Song, P., Russell, C. T., and Gary, S. P. (1994). Identification of low-frequency fluctuations in the terrestrial magnetosheath. *Journal of Geophysical Research: Space Physics*, 99(A4):6011–6025.

Sonnerup, B. U. O. (1969). Acceleration of particles reflected at a shock front. *Journal of Geophysical Research (1896-1977)*, 74(5):1301–1304.

Stawarz, J. E., Vasquez, B. J., Smith, C. W., Forman, M. A., and Klewicki, J. (2011). Third moments and the role of anisotropy from velocity shear in the solar wind. *The Astrophysical Journal*, 736(1):44.

Tao, C., Sahraoui, F., Fontaine, D., Patoul, J., Chust, T., Kasahara, S., and Retinò, A. (2015). Properties of Jupiter's magnetospheric turbulence observed by the Galileo spacecraft. *Journal of Geophysical Research (Space Physics)*, 120(4):2477–2493.

Trotignon, J. G., Mazelle, C., Bertucci, C., and Acuña, M. H. (2006). Martian shock and magnetic pile-up boundary positions and shapes determined from the Phobos 2 and Mars Global Surveyor data sets. *Planetary and Space Science*, 54(4):357–369.

Tu, C. Y. and Marsch, E. (1991). A case study of very low cross-helicity fluctuations in the solar wind. *Annales Geophysicae*, 9:319–332.

Turc, L., Roberts, O. W., Verscharen, D., Dimmock, A. P., Kajdič, P., Palmroth, M., Pfau-Kempf, Y., Johlander, A., Dubart, M., Kilpua, E. K. J., Soucek, J., Takahashi, K., Takahashi, N., Battarbee, M., and Ganse, U. (2023). Transmission of foreshock waves through Earth's bow shock. *Nature Physics*, 19(1):78–86.

Vörös, Z., Zhang, T. L., Leaner, M. P., Volwerk, M., Delva, M., and Baumjohann, W. (2008a). Intermittent turbulence, noisy fluctuations, and wavy structures in the Venusian magnetosheath and wake. *Journal of Geophysical Research (Planets)*, 113(E12):E00B21.

Vörös, Z., Zhang, T. L., Leubner, M. P., Volwerk, M., Delva, M., Baumjohann, W., and Kudela, K. (2008b). Magnetic fluctuations and turbulence in the Venus magnetosheath and wake. *Geophysical Research Letters*, 35(11):L11102.

Wang, J., Yu, J., Chen, Z., Xu, X., Li, K., Cui, J., and Cao, J. (2023). MAVEN Observations of Whistler-mode Waves Within the Magnetic Dips in the Martian Ionopause/Ionosphere. *The Astrophysical Journal*, 165(2):56.

Weber, T., Brain, D., Xu, S., Mitchell, D., Espley, J., Halekas, J., Mazelle, C., Lillis, R., DiBraccio, G., and Jakosky, B. (2020). The influence of interplanetary magnetic field direction on martian crustal magnetic field topology. *Geophysical Research Letters*, 47(19):e2020GL087757. e2020GL087757 10.1029/2020GL087757.

Wei, H. Y., Cowee, M. M., Russell, C. T., and Leinweber, H. K. (2014). Ion cyclotron waves at mars: Occurrence and wave properties. *Journal of Geophysical Research: Space Physics*, 119(7):5244–5258.

Wei, H. Y. and Russell, C. T. (2006). Proton cyclotron waves at mars: Exosphere structure and evidence for a fast neutral disk. *Geophysical Research Letters*, 33(23):L23103.

Wei, H. Y., Russell, C. T., Zhang, T. L., and Blanco-Cano, X. (2011). Comparative study of ion cyclotron waves at mars, venus and earth. *Planetary and Space Science*, 59(10):1039–1047.

Yamauchi, M., Hara, T., Lundin, R., Dubinin, E., Fedorov, A., Sauvaud, J.-A., Frahm, R. A., Ramstad, R., Futaana, Y., Holmstrom, M., et al. (2015). Seasonal variation of martian pick-up ions: Evidence of breathing exosphere. *Planetary and Space Science*, 119:54–61.

Zimbardo, G., Greco, A., Sorriso-Valvo, L., Perri, S., Vörös, Z., Aburjania, G., Chargazia, K., and Alexandrova, O. (2010). Magnetic Turbulence in the Geospace Environment. *Space Science Reviews*, 156(1-4):89–134.